EUROPEAN ORGANIZATION FOR NUCLEAR RESEARCH
European Laboratory for Particle Physics

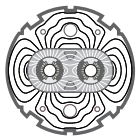

Large Hadron Collider Project

LHC Project Report 502

Contributions of the SL division to the workshop on beam-beam effects at Fermilab, June 2001

H. Grote, W. Herr, J.P. Koutchouk, Y. Luo, F. Schmidt, and F. Zimmermann
SL Division, CERN, 1211-Geneva 23

Abstract

This is a compilation of the papers and presentations contributed to the workshop on beam-beam effects, held from 25.-28.6. 2001 at Fermilab, Batavia, Illinois, U.S.A.

Administrative Secretariat
LHC Division
CERN
CH-1211 Geneva 23
Switzerland

Geneva, 8 October 2001

Beam-beam issues in the LHC and relevant experience from the SPS proton antiproton collider and LEP

W. Herr CERN, SL Division

Abstract

The beam-beam effects observed in SPS and LEP in various operational modes are reviewed. Special emphasis is put on effects relevant for the LHC. This includes orbit effects, crossing angle and PACMAN effects.

1 INTRODUCTION

In the LHC we have to expect numerous effects due to the beam-beam interactions. It is worthwhile to consider the experience gained running the SPS collider and LEP and use it in LHC studies where relevant knowledge is available [1, 2, 3]. The SPS was run approximately 10 years as a proton antiproton collider and the first hadron collider where long range beam-beam effect became important. LEP as an electron positron collider is very different from the LHC. The strong damping at its highest energy of 94.5 GeV allows beam-beam strength parameters up to 0.075, i.e. approximately 20 times larger than the expected values for the LHC of around 0.0034.

In SPS and LEP the two colliding beams had unlike signs, i.e. they travel in the same vacuum chamber on (a priori) identical orbits. However, both machines were run in various modes of operation and some of the observed features can be found again in the LHC, such as:

- Parasitic crossings for all modes of operation
- Orbit effects due to beam-beam kicks
- Effects from bunch trains
- PACMAN effects due to different types of beam-beam interactions
- Strong-strong beam-beam effects
- Coherent beam-beam effects
- Crossing angles

One can therefore hope that the concepts developed and tested for SPS and LEP can be applied to the LHC.

2 LHC LAYOUT

The conceptual layout of the LHC is shown in Fig.1. The two beams travel in two separate rings and cross over in the four experimental areas in interaction regions 1, 2, 5 and 8. To avoid unwanted interactions, crossing angles are used in these areas. To compensate first order long range effects, the crossing takes place in the horizontal plane in interaction regions 5 and 8 and the crossings in 1 and 5 are in the vertical plane.

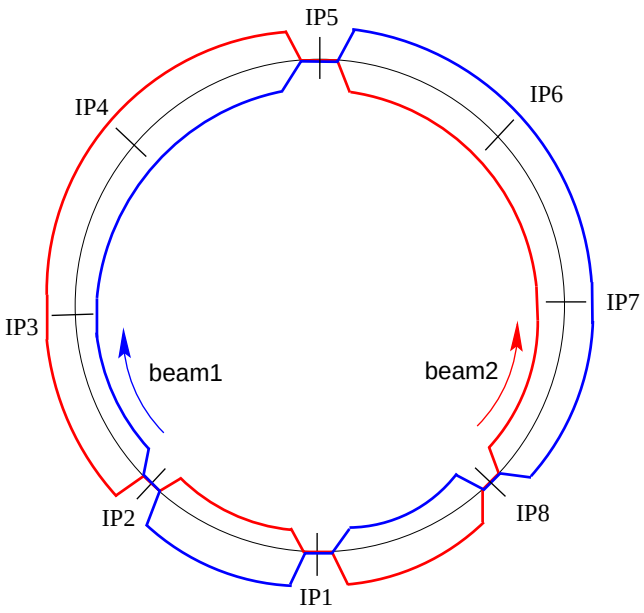

Figure 1: *Layout of LHC beams and collision points.*

3 SPS, LEP AND LHC PARAMETERS

A comparison of the most important SPS, LEP and LHC parameters is made in Tab.1. A few significant differences can be seen from Tab.1. The number of bunches per beam in the LHC is orders of magnitude larger than in SPS or LEP and consequently also the number of parasitic encounters. The damping time in both hadron machines, SPS and LHC, can be neglected compared to the very fast damping time in LEP of less than 4 ms at its highest energy. Another feature of the LHC is a finite crossing angle that is required to separate the beams. In SPS and LEP the crossing angles were unintentional and very small, except in dedicated experiments. The number of experiments is comparable and the 2+(1) for the SPS indicates 2 experimental areas plus one unavoidable head on collision. The SPS collider was also operated with 3 bunches per beam without separation, i.e. 6 head on collisions, but this mode of operation will not be considered here since it is not relevant for LHC studies.

Table 1: *Comparison of SPS, LEP and LHC parameters at high energy in collision*

	SPS	LEP	LHC
Bunches per beam	6	4 - 16	2808
Experiments	2+(1)	4	4
Parasitic interactions	9	4 - 28	120
ΔQ (ξ)/ IP	0.0050	0.0450 (0.0700)	0.0033
Damping time	-	0.004 s	10^5 s
Full crossing angle α	small	small	300 μrad

4 SPS AND LEP MODES OF OPERATION

4.1 SPS operation with pretzel scheme

When the SPS collider was operated with 6 bunches per beam, a horizontal pretzel scheme was used to separate the beams at the unwanted collision points (Fig.2). This pretzel extended over 5 of the 6 sectors and allowed head on collisions in the two main experiments UA1 and UA2 and an unwanted head on collision in between. During colliding beam conditions the beams were separated by about 6 σ at the unwanted collision points. For injection a single separator created a orbit distortion around the whole ring providing separation between 1.5 to 6 σ at the 12 crossing points.

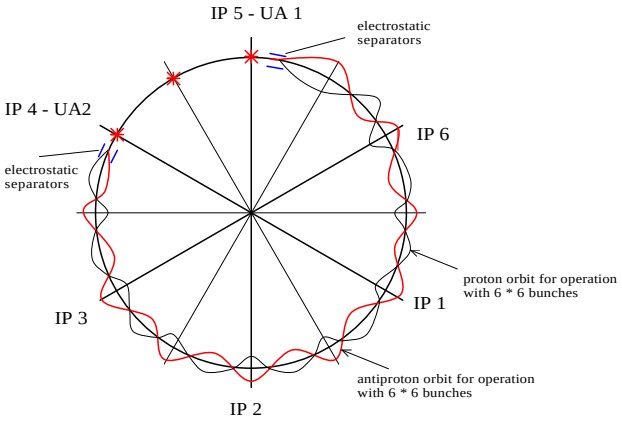

Figure 2: *SPS operation with horizontal pretzel scheme and 6 bunches per beam.*

4.2 LEP operation with bunch trains

During the last 6 years of its operation, LEP operated with bunch trains and although it also successfully used a horizontal pretzel scheme with 8 bunches per beam, I shall concentrate on its operation with bunch trains since this scenario gives more information relevant for the LHC.

To allow more than eight bunches per beam, a bunch train scheme was developped and installed in LEP [17, 18]. The basic idea is to start from the original four bunch scheme and to replace a single bunch by a short train of bunches. This requires a local separation at the unwanted collisions around the nominal collision point. A horizontal crossing angle was abandoned for background considerations and a local vertical separation was installed, using already existing separators in the interaction area. The principle of this mode of operation is shown in Fig.3.

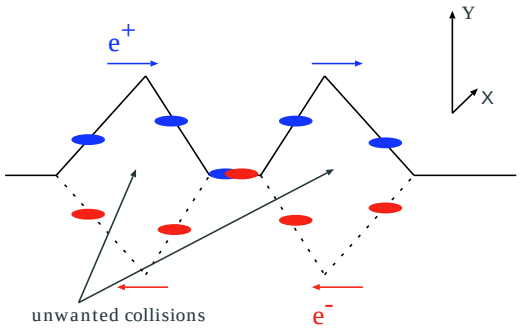

Figure 3: *Principle of bunch train separation in LEP.*

5 HEAD-ON BEAM-BEAM EFFECTS

The most basic beam-beam effects are due to the (wanted) head on collisions. Some of the results from the SPS collider are worth mentioning here. The working diagram of the SPS together with the tune footprints is shown in Fig.4. At injection energy the tune spread of the protons is dominated by the space charge tune spread of about $\Delta Q_h \approx -0.03$ and $\Delta Q_v \approx -0.05$ which is much larger than their beam-beam tune spread. The tune spread of the antiprotons is mainly due to the beam-beam effects from the protons and has opposite sign (Fig.4). In collision the total spread was about 0.015 to 0.018 and the life time was limited by high order beam-beam resonances since the footprint in collision is crossing the 13th and 16th order resonances. This is true in particular when the beam sizes of the two beams were not equal.

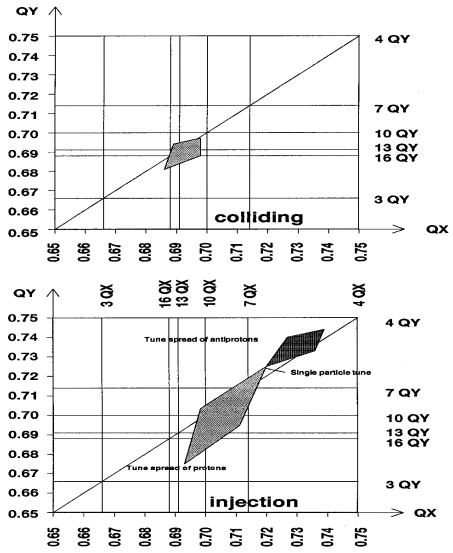

Figure 4: *SPS working diagram at injection and in collision.*

5.1 Unequal beam sizes

Without damping, the emittances of protons and antiprotons are determined by the injectors. On a single occasion, the emittances of the three antiproton bunches (X, Y, Z) were significantly different. It was noticed that the bunch with the largest emittance had a lower lifetime, suggesting a loss of particles from the tails of the distribution (Fig.5). After these large amplitude particles were lost, the lifetimes

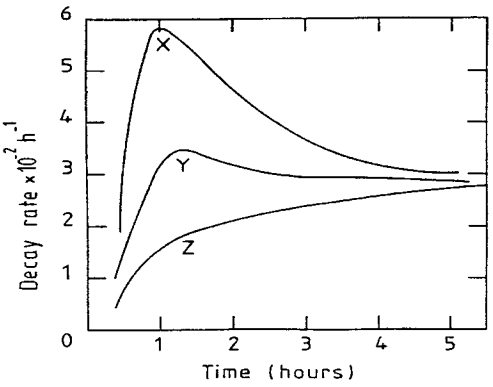

Figure 5: *Decay rate for antiprotons with unequal beam size.*

of the bunches became similar. The antiproton emittances were typically a factor two smaller ($\epsilon^* \approx 3$ mm mrad) than the emittances of the protons ($\epsilon^* \approx 6$ mm mrad). The large amplitude particles of the proton bunches now oscillate in the very non-linear part of the antiproton beam-beam force and are more sensitive to high order resonances. In

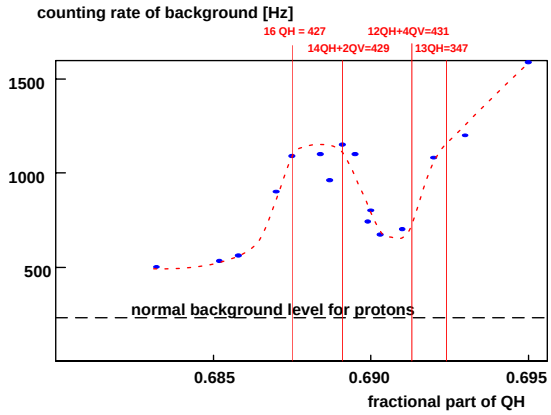

Figure 6: *Resonance scan across 13th and 16th order resonances in the SPS.*

the Fig.6 the result of a resonance scan is shown and the proton losses correlate with the 13th and 16th order resonance. This demonstrates the importance of resonances of very high order under such conditions. In another, dedi-

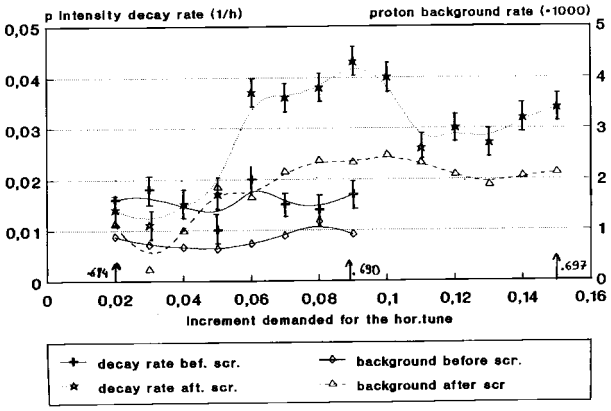

Figure 7: *Tune scan with protons before and after scraping of antiprotons.*

cated experiment the decay rate of a single proton bunch was measured and shown in Fig.7 as a function of the proton tune for two different sizes of the antiproton bunch (before and after scraping to smaller emittance). While for approximately equal beam sizes no significant effect is visible, the decay rate increases strongly in the neighbourhood of the 16th order resonance when the size of the antiproton bunch was decreased. The protons at large amplitudes experience now the very non-linear beam-beam force of the antiprotons and high order resonances are excited.

In the LHC we have to expect bunch to bunch emittance variations and for the reasons explained above they must be kept as small as possible. We presently allow a 10%

variation in our calculations.

5.2 *Dynamic β effects*

The beam-beam force changes the β-function at the collision point and as a result the optics is modified. The real tune shift ΔQ depends on this 'dynamic β' effect which depends on the optical parameters. Only in the limit of small values of the beam-beam parameter ξ and for tunes well above the integer the tune shift can be approximated by ξ. During the last few years of LEP operation this dynamic β effect became important. The unperturbed beam-beam parameter was in the order of 0.07 to 0.08 per interaction point and the phase advance between two interaction points was just above the integer (fractional tune 0.19 and 4 interaction points). The actual tune shift was therefore in the order of 0.04 [4]. The beating introduced around the machine was rather substantial leading to a reduction of β^* from 5 to $\approx$2.5 cm. Together with small phase advance errors (a few degrees are sufficient) between the interaction regions, a substantial difference of β^* between the interaction points has to be expected, and was manifested in a regularly observed luminosity imbalance between the four experiments. With the nominal parameters a noticable dynamic β effect is not expected in the LHC.

5.3 *Synchrobetatron resonances*

The finite crossing angle or a non-zero dispersion at the collision point can couple the longitudinal and transverse motion via the beam-beam interaction. This leads to the excitation of synchro-betatron resonances. The strength of the coupling due to a crossing angle can be expressed through the normalized crossing angle (or Piwinski angle) which is $\frac{\alpha \cdot \sigma_s}{2\sigma_z} \approx 0.7$ for the nominal crossing angle of 300 μrad for the LHC. Resonances of the type nQ_x+$mQ_y \rightarrow nQ_x$+mQ_y+rQ_s are excited and should show as additional lines in the tune spectrum. The effect of the crossing angle was simulated [5] and a tune scan with and without a crossing angle is shown in Fig.8. This simulation shows the appearance of synchrotron sidebands next to the main resonance lines but also a new resonance can be observed. For a strictly head-on beam-beam collision of round beams only even order resonances can be excited due to the symmetry of the system. This symmetry is broken either by long range interactions or by a crossing angle as demonstrated in Fig.8. The Fig.9 shows a similar scan but now for a non-zero dispersion at the collision point (D_x = 0.10 m). It can be derived [5] that a residual dispersion of 0.10 m is equivalent to a crossing angle of 300 μrad, i.e. excites synchro-betatron resonances with the same strength. Although these resonances have to be expected in the LHC, the synchrotron tune (Q_s = 0.00212) is very small compared to lepton accelerators (e.g. LEP Q_s = 0.10) and therefore the sidebands are very close to the main resonance line. The required space in the tune diagram is therefore hardly increased.

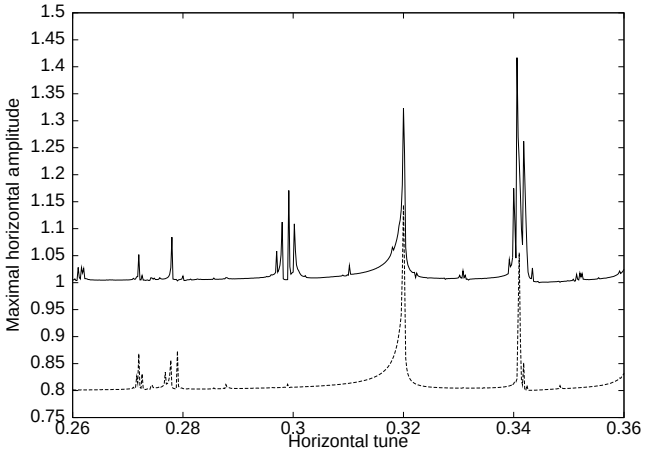

Figure 8: *Simulation of synchrobetatron resonances due to finite crossing angle.*

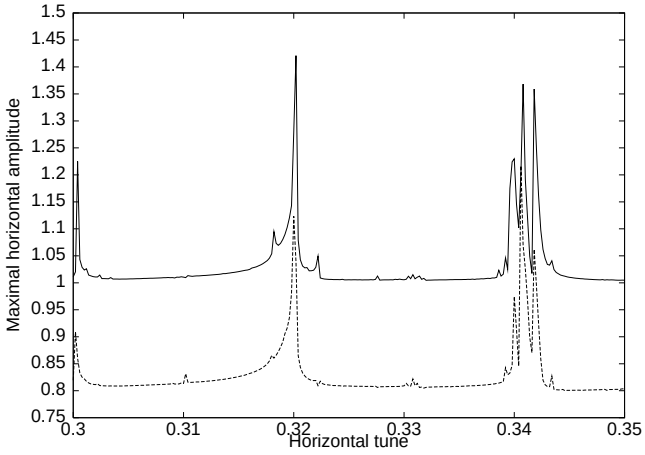

Figure 9: *Simulation of synchrobetatron resonances due to finite dispersion at interaction point.*

6 LONG RANGE BEAM-BEAM EFFECTS

Around the experimental regions the LHC beams travel in a common vacuum chamber and therefore experience the fields of the opposing beams, so-called long range interactions. The number of these parasitic encounters depends on the lengths of the common regions before the beams are sufficiently separated by dipole magnets and the bunch spacing. For the LHC we calculate 15 long range interactions on either side of the four collision points, i.e. we have approximately 120 distant interactions.

The effect of these interaction depends mainly on the separation, normalized to the transverse beam size. It can be shown that in the drift space between the collision point and the first focussing element this normalized separation

is constant:

$$d_{sep} \approx \frac{\alpha\beta^*}{\sigma^*} = \frac{\alpha\sqrt{\beta^*}\sqrt{\gamma}}{\sqrt{\epsilon^*}} = const. \qquad (1)$$

The long range interactions are therefore most important in the high luminosity, i.e. low β^* interaction regions. Although increasing the crossing angle α can improve the separation easily, other considerations have to be taken into account which limit this angle. Too large angles reduce the luminosity, require more aperture, strongly excite synchro-betatron resonances and bring the beams into the more non-linear part of the quadrupole fields of the insertion magnets. The present crossing angle of 300 μrad is a compromise between the different requirements.

6.1 Beam separation

To provide the required crossing angles, dedicated dipole magnets are used which act either on both or individual beams [6, 7]. An example of such a crossing angle bump is given for one beam in Fig.10. The orbit of the counter-rotating beam is antisymmetric around the central collision point. During injection, the beams are also separated in

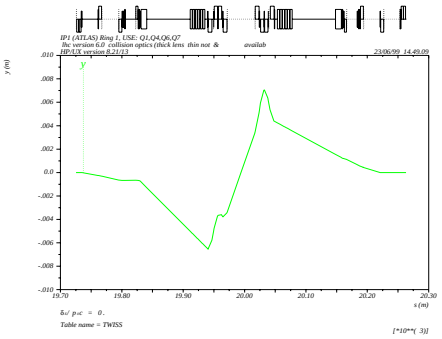

Figure 10: *Vertical bump for crossing angle.*

the second plane by a parallel bump of a few mm, ensuring that the normalized separation is never smaller than approximately 14 σ. Such a parallel bump is shown in Fig.11.

6.2 Dynamic aperture

The beam-beam effects decrease the available dynamic aperture of the LHC beams at injection and in collision, either alone or in combination with the non-linearities of the LHC lattice. Since this subject is treated in a different presentation [13] as well as simulations of the improvement of the dynamic aperture [14] using a long range compensation scheme [15], I do not give details on that subject in this report.

6.3 PACMAN effects

An effect which is expected to play a very important role is caused by the bunch filling pattern of the LHC, leading to

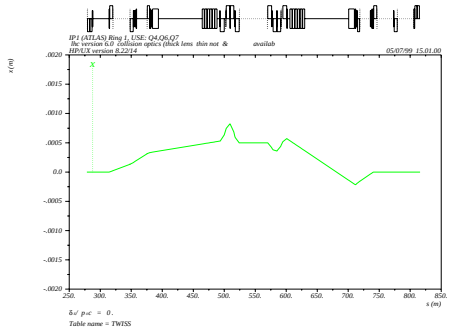

Figure 11: *Horizontal bump for parallel bump at injection.*

so-called PACMAN effects. The nominal bunch filling pattern of the LHC is shown in Fig.12. The pattern exhibits a

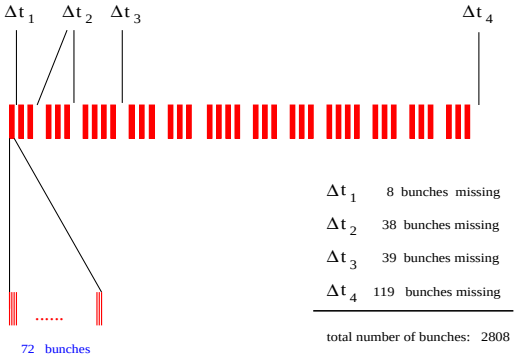

Figure 12: *Bunch filling scheme for the LHC.*

fourfold symmetry and has 39 batches of 72 bunches each, i.e. in total 2808 bunches of a maximum possible of 3564 are filled. The gaps between the batches are required for the injection and extraction kickers of the LHC injectors and a large gap at the end is needed to allow for the rise-time of the kicker of the beam dumping system. Ideally

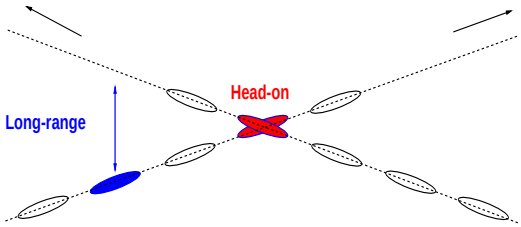

Figure 13: *Origin of PACMAN effects.*

the holes in the bunch train of one beam should meet holes of the other beam. This is true for the head-on collisions in interaction points 1 and 5. However the bunches at the beginning and end of a batch miss long range interaction either before or after the head-on collision (see Fig.13). This

left-right asymmetry cannot be avoided. In the worst case, i.e. for the first or last bunch of a batch, only half of the long range interactions are encountered [16]. Furthermore, in collision points 2 and 8 the large dump gap will meet a full batch and reduce the number of long range collisions of some bunches further. The maximum and minimum numbers of parasitic encounters become 120 and 40, respectively. Due to this gap some bunches will miss also head-on collisions. The interaction point 8 is moved longitudinally by 3 half bunch spacings, adding further missing head-on collisions to the interaction schedule and leaving bunches with only 2 out of 4 nominal head-on collisions. It is clear that all these bunches experience a very different accumulated beam-beam effect which may lead to different dynamics and, in the worst case, different life times. For beam measurements it is also important to have a reproducible reference and ideally one should use the nominal bunches.

To evaluate the strength of beam-beam interactions, a standard tool is to compute the tune footprint, i.e. the two dimensional tune shift as a function of the amplitude. Such footprints are shown in Fig.14 where I show the foot-

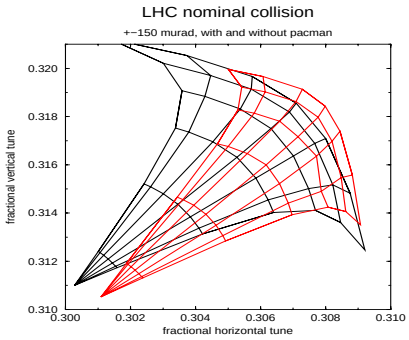

Figure 14: *Footprints for head-on and long range interactions for nominal (black) and PACMAN bunches (red).*

print for nominal bunches (i.e. bunches with all head-on and long range interactions) and the extreme PACMAN bunches (i.e. minimum number of long range interactions). The footprints are computed for the nominal parameters and bunch intensities. Although not visible, the effect of alternating horizontal and vertical crossing is all important since they compensate for the first order tune shift [1]. With all crossings in one plane the footprint of PACMAN bunches would be shifted rather far from the nominal and thus produce a very large operational tune spread. The bunches with one or more missing head-on collisions do not show in Fig.14 since for those the overall head-on part of the footprint just scales down and is therefore inside the nominal area.

6.4 *PACMAN effects with bunch trains in LEP*

It can be shown that operating LEP with bunch trains exhibits all properties of PACMAN effects. The separated

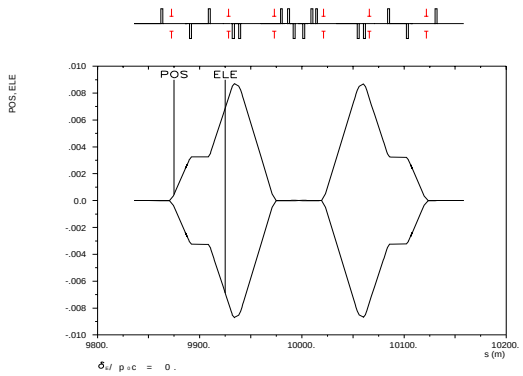

Figure 15: *Vertical separated orbits for bunch train operation around IP 4 for 45.6 GeV and central collision*

orbits of electrons and positrons around an experimental region is shown in Fig.15. While the central collision is head-on, the parasitic encounters have to be accommodated inside the separation bumps (Fig.15). This determines the parameters such as bunch spacing and number of bunches per train. The design allows a maximum of four bunches per train, spaced by 87 RF wavelengths, i.e. three parasitic collisions have to fit into the separation bumps on each side.

The left half of such a bump in an experimental region is shown again in Fig.16 together with the position of the parasitic encounters and the separation, normalized to the local horizontal beam size σ_x. The central collision point is at the right hand side of the figure and the horizontal axis gives the distance from the collison point. The figure

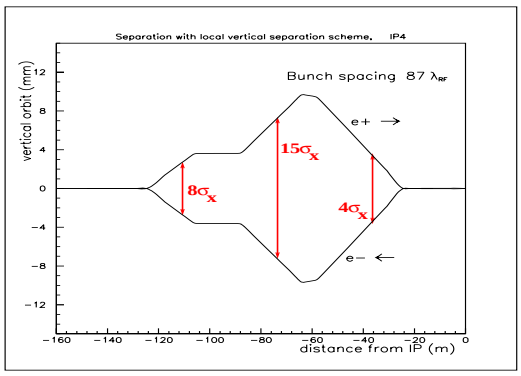

Figure 16: *Vertical separated orbits and normalized separation for bunch train operation around IP 4*

shows the situation when the bunches collide in the centre and for 45.6 GeV. For injection, the central collision has to be separated as well, imposing some constraints on the choice of the separation scheme. It further has to allow the fine adjustment of the head-on collision. Contrary to the

Table 2: *Separation and parasitic beam-beam strength ξ for parasitic collisions around IP 4 (for: ϵ_x = 30 nm, I_b = 500 μA)*

	3	2	1
d/σ_x	≈ 8	≈ 15	≈ 4
ξ_x (10^{-3})	$\approx$ 0.8	$\approx$ 0.2	$\approx$ 3.6
ξ_y (10^{-3})	$\approx$ -4.8	$\approx$ -0.7	$\approx$ -0.3

four bunch case, the separation bumps cannot be switched off during physics fills. The separation and the parasitic beam-beam tune shift is summarised for the three parasitic collisions in Tab.2. A horizontal emittance of 30 nm and a bunch current of 500 μA was used for the calculation. It is shown that in particular the outmost collision point gives the largest vertical tune shift while the other encounters give significantly smaller values. The Fig.17 and Tab.3

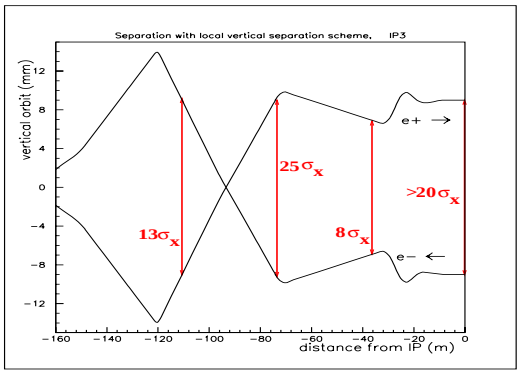

Figure 17: *Vertical separated orbits and normalized separation for bunch train operation around IP 3*

Table 3: *Separation and parasitic beam-beam strength ξ for parasitic collisions around IP 3 (for: ϵ_x = 30 nm, I_b = 500 μA)*

	3	2	1	0
d/σ_x	≈ 13	≈ 25	≈ 8	≥ 20
ξ_x (10^{-3})	$\approx$ 0.3	$\leq$ 0.1	$\approx$ 0.7	$\approx$ 0.1
ξ_y (10^{-3})	$\approx$ -0.2	$\approx$ -0.5	$\approx$ -0.2	$\approx$ -0.1

show the bump and tune shifts for a typical unused (i.e. odd) interaction region. The interaction at the central collision point is now also avoided. The separations are generally larger and the tune shifts smaller than for the experimental (even) regions. We therefore expect more problems from the parasitic encounters in the even than in the odd points.

Interaction schedule For four equal bunches and a high degree of symmetry of the optical layout of LEP, all bunches experience practically the same beam-beam effects. For not equally spaced bunches or finite bunch trains the interaction schedule can become rather complex. The extreme case of LHC with closely spaced bunches and gaps of different sizes leads to so-called PACMAN bunches [16] with a very complicated interaction schedule. The scheme with bunch trains in LEP shows a similar behaviour, although with fewer bunches. While the first bunch of a train has a head-on collision followed by the three parasitic encounters shown in Fig.16, the second bunch will first experience a parasitic encounter on the incoming side, followed by the head-on collision and two parasitic encounters on the outgoing side of the interaction point. Similar considerations can easily be made for all bunches of a train. As a consequence of this schedule every bunch of a train has a different sequence of beam-beam interactions and therefore experiences different effects. Some bunches may have very unfavourable encounters, e.g. those with small separation, and are likely to be most sensitive to unstable behaviour. One can therefore identify at least four different classes of bunches according to their beam-beam interactions, showing a "PACMAN-like" effect *within the beams*. In addition to the differences within a train, a residual non-closure of the separation bumps due to imperfections or energy mismatch causes a global offset that needs correction at each interaction point and can cause additional parameter splits *between the beams*.

Offsets and orbit separation The beam-beam kicks of the parasitic interactions distort the orbits of the individual bunches and since the collision pattern is different for different bunches, the orbits of all bunches are slightly different. As a consequence, the orbits at the interaction points are different and the bunches collide with a small offset. In the design of the bunch train separation scheme care was taken to make use of possible compensation effects to reduce these unwanted offsets [17, 18]. However, small offset of the order of μm are unavoidable. Furthermore, the orbit at the parasitic encounters itself is changed by the beam-beam kicks and a self-consistent calculation is required to give the correct answer. A program TRAIN was developped [19] to compute the individual orbits of all bunches in a train and the relevant parameters, such as tune, chromaticity, dispersion, offsets and crossing angles. The

Table 4: *Orbit offsets and separation (at central collision point) for 300 μA per bunch at 45.6 GeV*

	a	b	c	d
e^+ [μm]	+5.75	+1.10	-1.65	-0.30
e^- [μm]	+0.30	+1.65	-1.10	-5.75
d [μm]	+5.45	-0.55	-0.55	+5.75

orbit offsets and resulting separation of a train with four bunches is shown in Tab.4 for an experimental interaction point. An antisymmetry between the forward and backward beam can be observed as expected. The calculated separation amounts to more than the vertical r.m.s. beam size and it is clear that it is impossible to adjust the collision such that all bunches of a train collide head-on. The above example was computed for 45.6 GeV and bunch intensities of 500 μA, i.e. above what was actually achieved, but demonstrates the importance of this effect. The Fig.16

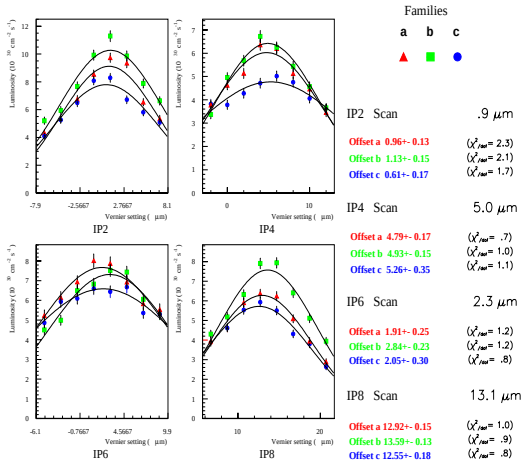

Figure 18: *Result of separation scans for three bunches per train*

shows the result of a vertical separation scan with simultaneous measurements of the luminosity for three bunches per train, the preferred operational scenario in 1995. The maximum luminosity, i.e. full bunch overlap, is reached at different vertical positions for the three bunches within a train, in full agreement with the calculation.

For four bunches per train this information is not available since most of the time LEP was operated with three bunches per train, i.e. 12 bunches total. This small offset proved to be an important performance limitation and the best tune shifts obtained were always smaller than in previous years, leading to a performance that was lower than expected. Nevertheless, the optimization of the bunch overlap was essential for a good performance. It should be mentioned, that from symmetry considerations a running with two bunches per train is most favourable since the symmetry of the collision is fully restored and both bunches of the train can be collided head-on, although possibly in different vertical position.

In the LHC the calculation of self-consistent orbits would be necessary for almost 3000 bunches and it is not obvious whether this is feasible nor whether a self-consistent solution exists.

Tune and chromaticity splits Once the self-consistent orbits were calculated, this information was used to compute the tune and chromaticity of the individual bunches in a train. The result is summarized in Tab.5 where q indi-

Table 5: *Fractional tunes and chromaticities are split inside a train for 300 μA per bunch at 45.6 GeV*

	a	b	c	d
q_x	0.3548	0.3612	0.3613	0.3547
q_y	0.2127	0.2235	0.2234	0.2133
Q_x'	0.4526	0.5000	0.5025	0.4848
Q_y'	0.1872	-0.2218	-0.2259	0.0053

cates the fractional part of the tune and Q' the chromaticity. The example was computed for 300 μA per bunch and 45.6 GeV and four bunches per train. The maximum tune difference was up to 0.010 and the chromaticity difference 0.41 units in the vertical plane. This is a significant limitation to the operational parameter space for the optimization of the performance.

When the machine was operated with four bunches per train, some bunches always had a lower life time, usually those who experienced a beam-beam interaction at small separation. This was confirmed in dedicated tests.

6.5 *Closed orbit effects in the LHC*

The TRAIN program [19] originally developped for the maximum 16 bunches of LEP was re-written to handle two beams with almost 3000 bunches each. Furthermore it must be able to handle different optics for the two beams. Details about the algorithm and its performance can be found in [8].

For the nominal bunch filling scheme the horizontal offset in interaction point 1 (IP1) is shown in Fig.19. The off-

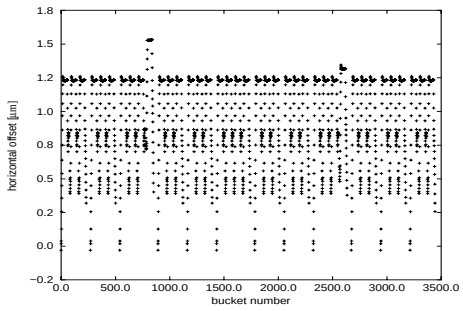

Figure 19: *Closed orbit along bunch structure in the LHC.*

set is shown in μm as a function of the bunch number, starting the count with the bunch following the large gap. The first bunch of beam one is assumed to collide with the first bunch of beam two in IP1. For symmetry reasons they also collide in IP5. In Fig.20 I show a zoom into the first part of Fig.19. Clearly visible are the nominal bunches in the middle of each batch (approximately 40). At both ends of

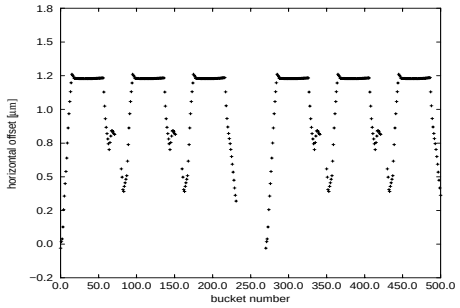

Figure 20: *Closed orbit along bunch structure in the LHC, zoomed into 3 batches.*

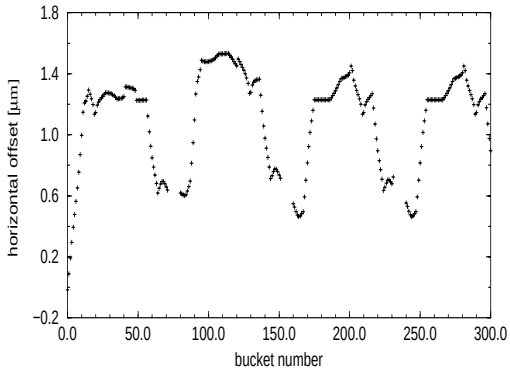

Figure 22: *Closed orbit along bunch structure in the LHC, zoomed into 3 batches. No fourfold symmetry.*

a batch the orbit offsets change due to the decreasing number of long range dipole kicks. The spread of the offset is in the order of 0.1 to 0.2 transverse beam sizes. Although this small offset has practically no effect on the luminosity, it needs to be studied whether quasi head-on collisions with a crossing angle and a small offset lead to an emittance growth or other unwanted side effects. In the Figs.21 and

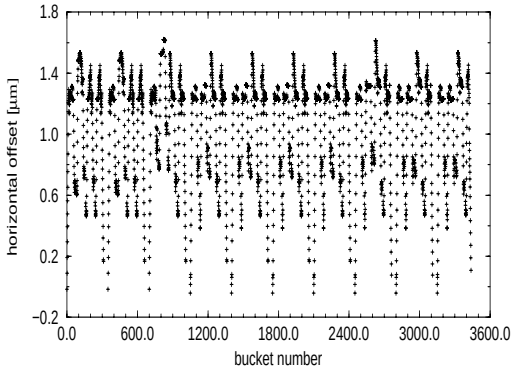

Figure 21: *Closed orbit along bunch structure in the LHC. No fourfold symmetry.*

22 I show similar data for an alternative filling scheme [9] which optimizes the number of bunches, however it does not have a fourfold symmetry. The effect is immediately visible: the offset is slightly increased but not dramatic, however practically no nominal bunches can be identified. This may lead to unwanted difficulties and uncertainties for beam measurements. As a further complication, we have to expect bunch to bunch intensity variations of 10 to 20%. In the TRAIN program this intensity variation can be considered and the result of such a variation is shown in Figs.23 and 24, again for the nominal filling scheme. The additional offset variation is clearly visible [9], and close to the acceptable level.

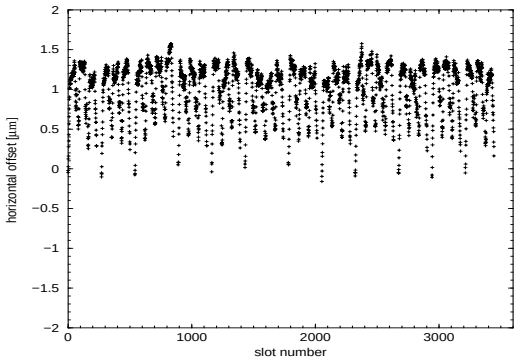

Figure 23: *Closed orbit along bunch structure in the LHC. 20% intensity variation between bunches.*

7 COHERENT EFFECTS

7.1 Coherent effects in LEP

Coherent beam-beam modes were frequently observed in LEP and due to the large beam-beam strength parameter the separation between the main modes, i.e. the σ- and π-mode is rather large allowing only a limited area in the tune space. Some background problems experienced in 1998 were attributed to the excitation of the horizontal π-mode near the half integer resonance. A clear demonstration of the two principal modes is shown in Fig.25 [20]. The tune spectra of two colliding bunches were recorded separately and the sum of the spectra is plotted. From the top to the bottom of the picture the phase of one spectrum is shifted in steps of one degree from zero to 360 degrees and the sum signal is shown. For zero and 360 degrees this corresponds to an in-phase signal and the σ-mode is be observed. For a phase difference of 180 degrees the out-of-phase signal corresponds to the π-mode. Both modes are very clearly visible, a clear demonstration that the modes observed at the corresponding frequencies can be associated to an in-phase and an out-of-phase motion of the two bunches.

A coherent quadrupole mode was observed once at LEP,

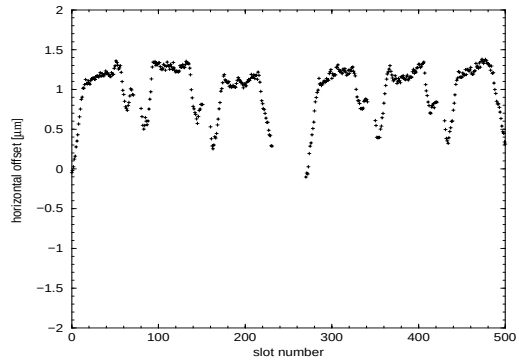

Figure 24: *Closed orbit along bunch structure in the LHC, zoomed into 3 batches. 20% intensity variation between bunches.*

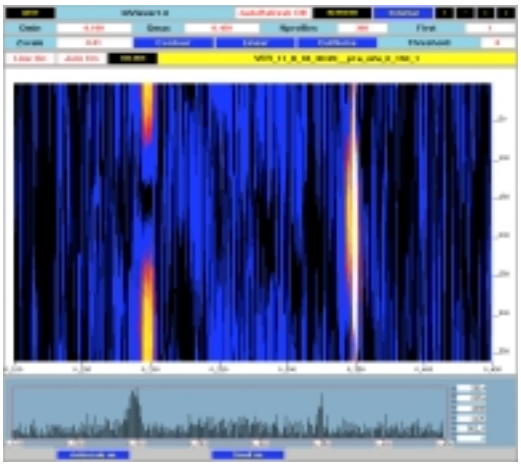

Figure 25: *Demonstration of coherent beam-beam modes in LEP*

however was never reproduced afterwards.

7.2 Coherent effects in LHC

Possible excitation of coherent dipole modes in the LHC were studied using new simulation techniques and details can be found in [10, 11, 12].

8 CONCLUSION

Amongst the numerous information on beam-beam effects we have obtained at LEP, some are of importance for the evaluation of LHC beam-beam effects although a quantitative application is not possible. The orbit effects caused by beam-beam kicks have been identified as a severe problem. A self-consistent treatment was vital to understand the observations quantitatively and the PACMAN like effects have limited the performance. The experience has shown that parameter splits between the beams or the bunches within a beam must be kept as small as possible and self-compensation of these effects must be used wherever possible in the design process.

9 REFERENCES

[1] W. Herr; *Experience with beam-beam effects in LEP* Proc. workshop on beam-beam effects in hadron colliders LHC99, (CERN, Geneva 1999) CERN SL/99-039 (AP) (1999) 7.

[2] R. Schmidt; *Beam-beam observations in the SPS proton antiproton collider* Proc. workshop on collective effects in large hadron colliders, (Montreux, 1994) Part. Accelerators Vol.**50**, Number 1-3, p. 47, (1995).

[3] K. Cornelis; *Beam-beam effects in the SPS proton antiproton collider* Proc. workshop on beam-beam effects in hadron colliders LHC99, (CERN, Geneva 1999) CERN SL/99-039 (AP) (1999) 2.

[4] D. Brandt, W. Herr, M. Meddahi and A. Verdier; *Is LEP beam-beam limited at its highest energy ?* Proceedings of 1999 Part.Acc.Conf., New York, 29.3.-2.4. 1999.

[5] L. Leunissen; *Influence of vertical dispersion and crossing angle on the performance of the LHC* Proc. workshop on beam-beam effects in hadron colliders LHC99, (CERN, Geneva 1999) CERN SL/99-039 (AP) (1999) 81.

[6] O. Brüning, W. Herr, R. Ostojic, *A beam separation and collision scheme for IP1 and IP5 at the LHC for optics version 6.1*, CERN LHC Project Report 315

[7] O. Brüning, W. Herr, R. Ostojic, *A beam separation and collision scheme for IP2 and IP8 at the LHC for optics version 6.1*, CERN LHC Project Report 367

[8] H. Grote; *Self-consistent closed orbits caused by beam-beam effects in the LHC* Proc. Europ. Part. Acc. Conf. 2000, (Vienna, 2000) 1202.

[9] H. Grote and W. Herr; *Self-consistent closed orbits caused by beam-beam effects in the LHC* Proc. this workshop, (FNAL, 2001).

[10] Y. Alexahin, H. Grote, W. Herr and M.P. Zorzano,*Coherent beam-beam effects in the LHC* Proc. International Conf. on High Energy Accel. HEACC 2001, (Tsukuba, 2001) and LHC Project Report 466 (2001).

[11] W. Herr, M.P. Zorzano and F. Jones; *Beam-beam simulations using a Hybrid Fast Multipole Method.* Phys. Rev. ST Accel. Beams **4**, 054402 (2001).

[12] W. Herr, M.P. Zorzano and F. Jones; *Beam-beam simulations using a Hybrid Fast Multipole Method.* Proc. this workshop, (FNAL, 2001).

[13] Y. Luo and F. Schmidt; *Beam-beam simulations for the LHC at injection and collision energies.* Proc. this workshop, (FNAL, 2001).

[14] F. Zimmermann; *Weak-strong simulation studies for the LHC long-rang beam-beam compensation.* Proc. this workshop, (FNAL, 2001).

[15] J.P. Koutchouk; *Correction of the Long-Range Beam-Beam Effect in LHC using Electromagnetic Lenses.* Proc. this workshop, (FNAL, 2001).

[16] W. Herr; *Effects of PACMAN bunches in the LHC*; CERN LHC Project Report 39 (1996).

[17] W. Herr; *Bunch trains without a crossing angle*; Proc. 4th workshop on LEP performance, (Chamonix 1994) CERN SL/94-06 (DI) (1994) 323.

[18] B. Goddard $et\ al.$; *Bunch trains for LEP*; Part. Accelerators Vol.**57**, Number 4, p. 237, (1998).

[19] E. Keil; *Truly selfconsistent treatment of the side effects with bunch trains*; CERN SL/95-75 (AP) (1995).

[20] G. Morpurgo; *Private communication*;

SELF-CONSISTENT ORBITS WITH BEAM-BEAM EFFECT IN THE LHC

H. Grote and W. Herr, CERN, Geneva, Switzerland

Abstract

In part of the straight sections of the LHC the two beams share a common beam tube. Therefore the bunches cross each other not only at the interaction point, but as well at many places on either side, with a typical transverse separation of 10 times the transverse beam size. These "parasitic" encounters lead to orbit distortions and tune shifts, in addition to higher order effects. Since the string of bunches from the injection machine contains gaps, not all possible 3564 "buckets" around the machine are filled, but only about 3000. This in turn causes some bunches to not always encounter bunches in the opposite beam at one or several parasitic collision points (so-called "pacman" bunches), or even at the head-on interaction point ("super-pacman" bunches). With a special program self-consistent orbits in the LHC have been calculated for the first time with the full beam-beam collision scheme resulting from various injection scenarios [1]. The offsets at the interaction points, and the tune shifts are shown to be small enough to be easily controlled.

1 INTRODUCTION

In the LHC [2] the two opposite beams share a common beam tube for roughly 50 m on either side of the four interaction points. Since the bunch spacing is only 7.5 m, in order to avoid unwanted head-on collisions the beams cross with an angle. Even so, in addition to the one head-on encounter at each interaction point there remain 15 positions on either side of it where the closed orbits at nominal energy are only about 10 σ apart, and even less in the focusing quadrupoles at either side of each interaction point. Various effects (alignment errors, field errors, momentum errors, imperfect injection, beam-beam kicks) may lead to significant orbit distortions and further distance reduction. Because of "holes" in the filling scheme the situation differs from bunch to bunch. The principal effects on the bunches caused by the beam-beam encounters are tune shifts and orbit offsets at the interaction points. The former are potentially dangerous because they may shift the tune of a bunch onto a resonance which may lead to its loss; the latter reduce the luminosity, and the offset at the head-on collision creates an extra orbit kick that adds to the distortions already present. Further possible causes for worry are changes in the chromaticity, non-zero dispersion at the interaction point, odd order resonances, and possibly higher order effects. The aim of the current study was therefore to see whether acceptable closed orbits exist for all bunches in both beams, whether the coherent tune shifts remain small enough to be of no concern, and the other effects mentioned can be corrected if necessary. The study provides as well input for the layout of the correction system in that it gives typical values for orbit errors caused by beam-beam effects.

The results are presented in graphical form because of the large number of bunches. The bucket number for ring-1 is constructed as follows: bucket number zero is at IP5, bucket number one to the left of it (seen from top), number two further to the left and so on backwards through IP4, IP3, IP2, IP1, IP8 etc. until to the right of IP5. The beam rotates clockwise. For ring-2 the numbering is done from IP5 to the right, the beam rotates anti-clockwise.

2 BUNCH FILLING SCHEME

72×1 8×0 72×1 8×0 72×1 38×0
72×1 8×0 72×1 8×0 72×1 38×0
72×1 8×0 72×1 8×0 72×1 8×0 72×1 39×0
72×1 8×0 72×1 8×0 72×1 38×0
72×1 8×0 72×1 8×0 72×1 38×0
72×1 8×0 72×1 8×0 72×1 8×0 72×1 39×0
72×1 8×0 72×1 8×0 72×1 38×0
72×1 8×0 72×1 8×0 72×1 38×0
72×1 8×0 72×1 8×0 72×1 8×0 72×1 39×0
72×1 8×0 72×1 8×0 72×1 38×0
72×1 8×0 72×1 8×0 72×1 38×0
72×1 8×0 72×1 8×0 72×1 119×0

Whatever the bunch filling scheme, as long as it is the same for both rings, and the injection is symmetric to IP1 and IP5, every bunch in ring-1 will collide with a bunch in ring-2 (and vice versa) at IP1 and IP5. For this to be true as well at IP2 and IP8, the following condition has to be fulfilled:

The distance from IP to IP is 891 half-buckets (bunches collide every half-bucket since both beams move) except for IP8 which is 888 from IP7 and 894 from IP1. The reason is the longitudinal displacement of IP8 with respect to the symmetry point. If the injection scheme repeats itself every 891 buckets, then at all IPs a bunch will always meet a bunch. Therefore super-pacman bunches are created at IP8 due to this displacement. The filling scheme shown here respects this symmetry almost fully, only at the end a batch of 72 bunches is missing to allow for the risetime of the beam dump kickers, creating super-pacman bunches at IP2 and IP8. In symbolic form it can be written as above (1 means bunch present, 0 absent).

3 ALGORITHM

The calculations are performed with two programs, MAD [3] and TRAIN, the latter being a heavily modified version

of the program TRAIN [4] developped for LEP. Both programs communicate via a database DOOM.

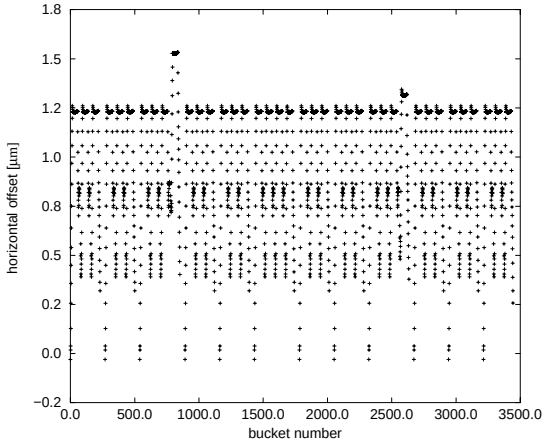

Figure 1: Horizontal offset at IP1 for all ring-1 bunches. The offset in caused exclusively by beam-beam interactions. The spread is about 1/10 of the beam size.

For the results presented here, a thin-lens model of the LHC version 6.0 was used, containing the latest separation and crossing schemes of version 6.1 [5], [6]. In the first step, the two LHC lattice and optics files are prepared for the TRAIN program: the lattice file for LHC ring-1 is read, the crossing and separation bumps are matched, tunes and chromaticities are adjusted, the places of head-on and parasitic encounters are marked, and the second order maps between all these beam-beam interaction points are lumped. This is justified since the optics under study contains only dipoles, quadrupoles, and sextupoles; field and alignment errors are not present. The Twiss parameters, element, lattice, force, and map tables are then stored in DOOM. The same procedure is followed using a matched thin-lens version for ring-2. At the end of this step, then, the database contains the necessary information for both rings to perform the self-consistent orbit finding.

This second step is performed by the program TRAIN. It first reads the description of the two rings from the database, and in particular the number and position of all beam-beam encounters. It then reads the injection schedule from an independent file and establishes the "encounter list" for all bunches in both beams. Next the program finds an initial closed orbit from the linear one-turn matrices with beam-beam encounters switched off. The program then iterates in a double loop over all bunches in both rings, with beam-beam encounters switched on. Where which bunch meets which bunch in the other ring is known from the bunch filling scheme. The inner loop is iterated with fixed distances between bunches at the beam-beam encounters, i.e. fixed beam-beam kicks. When it has converged to closed orbits for all ring-1 and ring-2 bunches, then the bunch positions at the beam-beam encounters are updated, and the outer loop is iterated until these positions do not change anymore. The bunch sizes are kept fixed as calculated from the undisturbed beta-functions, their change in size is negligible. Once all orbits (i.e. their six-dimensional initial coordinate vectors) are known, each bunch pair is tracked with the second order maps to get the tunes, chromaticity, and dispersion. The total CPU time for 2808 bunches in each beam is of the order of a few minutes on a fast workstation (e.g. Pentium III).

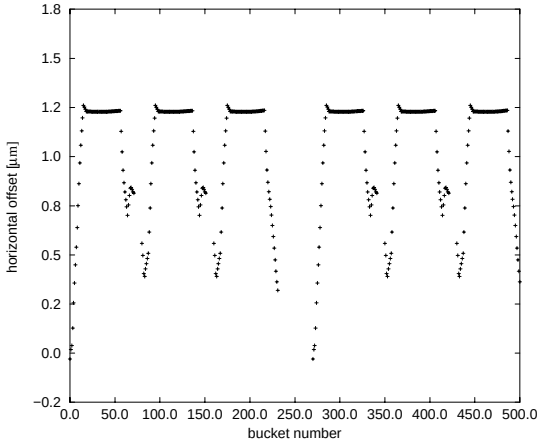

Figure 2: Detail of Figure 1. The 15 pacman bunches at either end of each bunch packet of 72 bunches can clearly be seen. The small irregularities are caused at IP2 and IP8.

4 COHERENT TUNES, CHROMATICITY, LUMINOSITY, AND DISPERSION

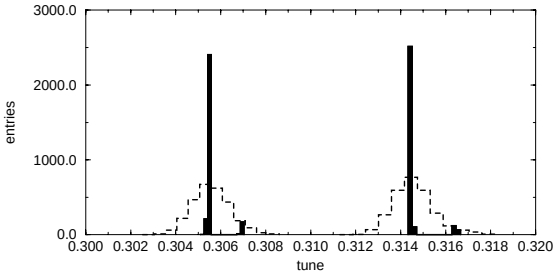

Figure 3: Solid: horizontal (left) and vertical tunes for all 2808 bunches in ring-1. The two offset bumps belong together. They represent the 186 super-pacman bunches occuring at IP8. Dashed: tune spread resulting from a Gaussian beam current distribution.

The coherent horizontal and vertical tunes for all bunches are shown in Figure 3. The offset batch stems from the super-pacman bunches at IP8; IP2 has practically no effect since there the beams are separated by about 4σ. The offset of the normal bunches is as expected, i.e. roughly $-3 \times 0.00342/2 = -0.0051$ (the undisturbed fractional tunes are 0.31 and 0.32, respectively). When the bunch currents in both rings have a Gaussian distribution rather than being equal as in the results presented up to now, this has very little effect on the orbit offsets, since they are

caused by over one hundred parasitic encounters and are thus averaged; however, there is a visible effect on the coherent tune shift which is caused by the head-on collisions only, of which there are up to three (the separation of 4σ at IP2 makes this head-on collision insignificant for the tune shift). Figure 3 shows the coherent horizontal tune shift resulting from a Gaussian bunch current distribution with $\sigma = 0.2\, c_{nom}$ ($c_{nom} = 0.189$ [mA] is the nominal bunch current). The spread doubles with respect to the case with fixed beam current, but is still within $\pm 2 \times 10^{-3}$ which is not dramatic. Bunch current variations of this order can therefore be tolerated, provided there are no other effects not studied here that give reasons for concern.

The change in the dispersion is below 1 mm for all bunches. The luminosity resulting from the offset at the collision points lies between 0.98 and 1 without correction. When the average offset (see Figure 2) is corrected, the overall luminosity drops by less than 0.001.

The horizontal and vertical chromaticity without beam-beam effect were adjusted to 1.6 and 1.8, respectively. The chromaticities with beam-beam effect are given in Figure 4. This effect can be tolerated since the range of acceptable chromaticities is between one and two.

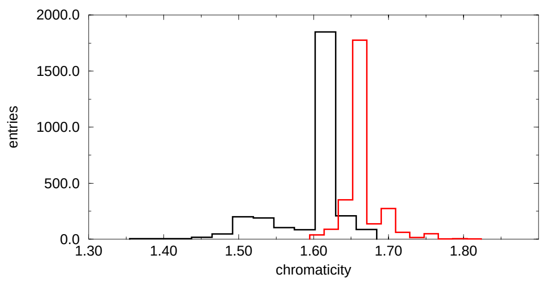

Figure 4: Horizontal (black) and vertical chromaticities for bunches in ring-1.

5 OTHER APPLICATIONS

The program TRAIN has some very important applications in the definition of LHC parameters. Various different filling schemes have been proposed, mainly to optimize the number of bunches and therefore the luminosity. However, possible implications of the filling scheme on the beam dynamics, in particular on the beam-beam induced orbits have been ignored or estimated on an averaged basis. This program now allows to test the different proposals and chose the most suitable one.

5.1 Test of alternative filling schemes

72×1	8×0	72×1	8×0	72×1	8×0	72×1	38×0
72×1	8×0	72×1	8×0	72×1	8×0	72×1	38×0
72×1	8×0	72×1	8×0	72×1	8×0	72×1	38×0
72×1	8×0	72×1	8×0	72×1	8×0	72×1	38×0
72×1	8×0	72×1	8×0	72×1	8×0	72×1	38×0
72×1	8×0	72×1	8×0	72×1	8×0	72×1	38×0
72×1	8×0	72×1	8×0	72×1	8×0	72×1	38×0
72×1	8×0	72×1	8×0	72×1	8×0	72×1	38×0
72×1	8×0	72×1	8×0	72×1	8×0	72×1	38×0
72×1	8×0	72×1	8×0	72×1	8×0	48×1	126×0

The bunch filling scheme defined above can provide the largest number of bunches (2856), but does not any more exhibit a fourfold symmetry, but rather a ten fold symmetry. That does not match the periodicity of the LHC layout and, although the luminosity is highest in the interaction points 1 and 5, the symmetry is strongly broken by interactions points 2 and 8, leading to a much more irregular structure. In particular the number of bunches missing head-on collisions is largely increased. This is

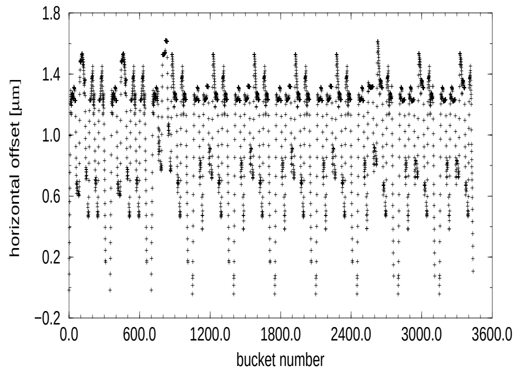

Figure 5: *Closed orbit along bunch structure in the LHC. No fourfold symmetry.*

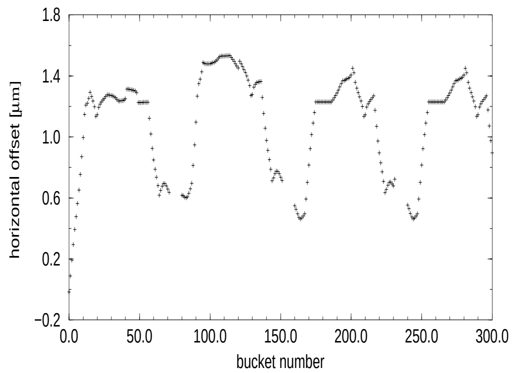

Figure 6: *Closed orbit along bunch structure in the LHC, zoomed into 3 batches. No fourfold symmetry.*

shown in Figs.5 and 6. Most important, it is difficult to identify nominal bunches (see Fig.6). This bunch filling scheme was discarded following these studies.

5.2 Effect of bunch to bunch intensity variations

Another effect can easily be studied using the TRAIN program. It allows to assign individual bunch intensities to all bunches of the train. The presently assumed bunch to

bunch variation is about 20%. The result of the calcula-

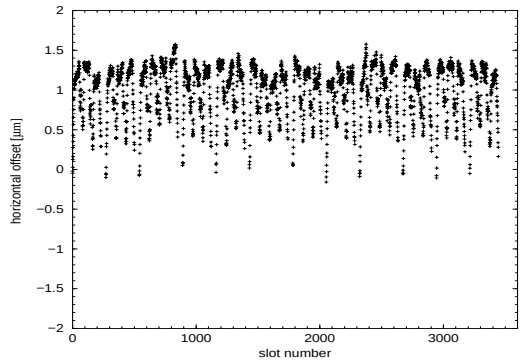

Figure 7: *Closed orbit along bunch structure in the LHC. 20% intensity variation between bunches.*

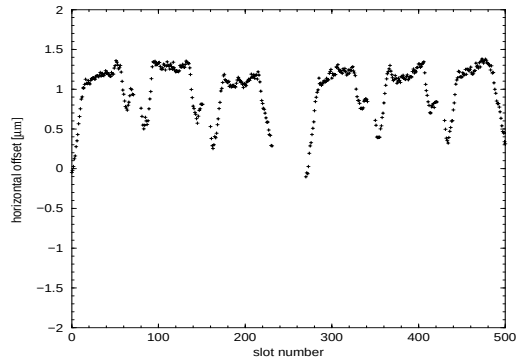

Figure 8: *Closed orbit along bunch structure in the LHC, zoomed into 3 batches. 20% intensity variation between bunches.*

tion is shown in Figs.7 and 8. Although the orbits are now all different for the originally nominal bunches, the variation is small (1 - 2% of the beam size).

6 CONCLUSIONS

The self-consistent bunch orbits presented here for the latest bunch filling scheme allow the following conclusions which of course concern only the closed orbits for zero phase-space amplitude, and not any other parameter such as long-term stability, lifetime, emittance blow-up, dynamic aperture etc.:

- The bunch offsets lie within $\pm 0.1\sigma$ at the physics collision points
- The effects on other parameters (tune, chromaticity, dispersion) are small, and their shifts can easily be corrected (not their spread)
- The algorithm allows to evaluate and decide on filling schemes
- The effect of bunch to bunch intensity variations can be studied

7 REFERENCES

[1] H. Grote, “Self-Consistent Orbits with beam-beam effect in the LHC”, Proc. of Europ. Part. Acc. Conf. 2000 (Vienna, 2000), 1202.

[2] The LHC Study Group, “The Large Hadron Collider - Conceptual Design”, CERN/AC/95-05

[3] H. Grote and F.C. Iselin, “The MAD Program”, CERN/SL/90-13 (AP) (Revision 3) (1992).

[4] E. Keil, “Truly Self-Consistent Treatment of the Side Effects with Bunch Trains”, CERN SL/95-75

[5] O. Brüning, W. Herr, R. Ostojic, “A beam separation and collision scheme for IP1 and IP5 at the LHC for optics version 6.1”, CERN LHC Project Report 315

[6] O. Brüning, W. Herr, R. Ostojic, “A beam separation and collision scheme for IP2 and IP8 at the LHC for optics version 6.1”, CERN LHC Project Report 367

A Hybrid Fast Multipole Method applied to beam-beam collisions in the strong-strong regime.

W. Herr, M.P. Zorzano, CERN, and F. Jones, TRIUMF

Abstract

The strong-strong interactions of two colliding beams are simulated by tracking the motion of a set of macroparticles. The field generated by each distribution is evaluated using the Fast Multipole Method (FMM) together with some elements of particle-mesh methods. This technique allows us to check the exact frequencies of the coherent modes and the frequencies of oscillations of individual particles in the beam. The agreement between the simulations and analytical calculations is largely improved. Furthermore it is an efficient method to study the coherent modes in the case of separated beams.

1 INTRODUCTION

Two colliding beams exert a force on each other which is defocusing for beams of equal polarity as in the case of the LHC. Solutions of the linearized Vlasov equation show that for round beams and in the case of one bunch per beam with equal parameters (intensity, beam size, betatron tune) two coherent dipole modes of oscillations appear: the σ mode, whose frequency is equal to the unperturbed betatron tune, and the π-mode with a tune shift of $Y = 1.21$, where Y is the Yokoya factor [1], times the beam-beam parameter ξ.

In this paper the transverse coherent motion of two colliding proton beams is studied by multiparticle tracking. In a self-consistent model of the coherent interaction, the distributions of both beams evolve as a consequence of the mutual interaction and are used at the interaction points to calculate the force on the individual particles. A number of studies have been done for LHC using the so-called "soft Gaussian model" [2]. This model assumes the force experienced by a particle when traversing the counter rotating beam as originating from a Gaussian beam distribution with variable barycenters and rms beam sizes. This allows the use of an analytical expression for the forces. This Gaussian model cannot take into account the non-Gaussian deformations of the distribution and as a result underestimates the force and yields a Yokoya factor that is slightly smaller ($Y = 1.1$ in our case). This symptom has also been recently discussed by Yokoya [3]. In the worst case this simplification can inhibit the appearance of coherent effects. Nonetheless the use of the analytical expression of the force generated by a Gaussian beam allows simulations in a reasonable computing time and it is therefore more convenient for studies with multiple bunches.

It has been predicted [4, 5] that the coherent π-mode may not be Landau damped for certain strong-strong conditions and therefore an accurate knowledge of the Yokoya factor is highly desirable.

2 SIMULATIONS BEYOND THE SOFT GAUSSIAN MODEL

To avoid this problem and to increase the accuracy of the simulations, we have to introduce a field solver for an arbitrary distribution of charges in space. The choice of the solver is constrained by the problems under investigation:

- Large number of particles in simulation (10^4).
- Separated beams (separation between zero and 10 times the beam size or more).

A direct integration of forces (particle-particle methods) is ruled out since the necessary time grows with the square of the number of particles (O(N_p^2)). For the number of particles used in our simulation this is impossible. Other possible solvers employ so-called particle-mesh methods and have been shown to give good results [6]. Their advantage is speed since the number of computations is smaller and depends on the number of grid points N_g: (O($N_g ln N_g$)). A strong disadvantage is that particle-mesh methods have problems handling non-uniform distributions. For the case of separated beams (as in our case with the important effect of long-range collisions) most of the space is basically empty. Moving or adaptive grids may be used for that purpose, but may lead to a rather complicated structure.

Another possibility is to use Fast Multipole Methods (FMM). In this algorithm the potential or force acting on a particle is divided into two components. The component of close particles is computed directly and between distant particles the potential is approximated by multipole expansion [7, 8]. This method is therefore well adapted to handle problems like separated beams. Problems with FMM are close encounters and "charge-overloading", i.e. for the LHC bunches 10^{11} particles are represented by 10^4 macroparticles.

3 BASIC HFMM ALGORITHM

For our problem we studied a modified version of FMM, a Hybrid FMM (HFMM) [9]. It resembles a particle mesh method for the handling of charges and super particles, however the forces on the superparticles are evaluated using the FMM. Smoothing can help to avoid charge-overloading. The HFMM is a robust implementation of a

Fast-Multipole Method (FMM) field solver, which is designed to solve the field for an arbitrary collection of discrete charges. It divides the solution domain into a grid and a halo area. The grid area is subdivided into a hierarchical tree of square regions. In the first step of the calculation, the macroparticles inside the grid are assigned to grid points. All macroparticles outside the grid are treated as discrete, independent superparticles and form the halo. The charge assignment can be done with a 'nearest-grid-point' method, i.e. the charge is assigned to the nearest grid point. This is the simplest method, however the field values are not continuous and the results are more noisy. Alternatively one can use the cloud-in-cell (CIC) charge assignment where the charge is shared between the neighbouring grids points. This method gives continuous field values but requires more book-keeping.

Finally, multipole expansions of the field are computed for every point, i.e. for each grid point as well as for every halo particle, and the program derives the resulting forces on the particles of the counterrotating beam. In the case of a CIC charge assignment, appropriate interpolation between the fields calculated for the grid points have to be applied. The grid size and shape does not have to follow any special geometry and can be chosen freely to achieve the desired speed and precision, depending on the problems under investigation. Unlike other Poisson solvers, the grid points with no charges assigned are left out of the computation and the number of computations scales roughly with the number of particles. More details of the method used in this report are found in [9]. This method is already implemented in the ACCSIM program [10] to study space charge problems.

In this work we have implemented the HFMM in our beam-beam simulation program to evaluate the force on a test particle generated by an arbitrary charge distribution. This will be applied to study the strong-strong collision of two bunches colliding at one interaction point (IP). We will study the coherent modes that are excited in the collision of two equal round bunches similar to those of LHC, when colliding head-on or separated by a constant offset at one interaction point (long-range interactions). This will enable us to obtain the correct Yokoya factor by multiparticle tracking and in a later stage to study in detail the modes excited by long-range interactions. Finally, it should allow us to study the possible emittance growth of collisions of partially overlapping bunches [11].

4 TRACKING WITH HFMM.

We simulate the collision of two strong proton beams. Our variables are: horizontal position x, vertical position y, horizontal angle $v_x = x'$, and vertical angle $v_y = y'$. The prime denotes the derivative with respect to longitudinal position s, *e.g.* x' is the slope of the horizontal trajectory.

Each of the beams has one bunch that is represented by a set of N_p macroparticles, whose trajectories are followed over n turns, assuming linear betatron motion without coupling and a beam-beam collision at one interaction point (IP). At the IP every particle in the bunch experiences a deflection by the field of the counter-rotating beam that depends on its position.

The deflection applied to a single particle in one of the beams is calculated using the HFMM.

The linear map from one IP to the next is

$$\begin{pmatrix} x(n+1) \\ v_x(n+1) \end{pmatrix} =$$

$$\begin{pmatrix} \cos(2\pi Q_x) & \sin(2\pi Q_x) \\ -\sin(2\pi Q_x) & \cos(2\pi Q_x) \end{pmatrix} \begin{pmatrix} x(n) \\ v_x(n) + \Delta v_x(n) \end{pmatrix} \quad (1)$$

An equivalent map is applied in the vertical plane, (y, v_y).

The horizontal deflection experienced at the interaction point is:

$$\Delta v_x(n) = \frac{r_p N^*}{\gamma} E_x(x, y) \quad (2)$$

where $E_x(x, y)$ is the horizontal force evaluated with the HFMM technique at the particle position (x, y). The number of particles in the opposing beam is N^*.

For the simulation of parasitic (long-range) collisions, the same model is employed. The two beams collide with a horizontal separation L_x (in units of σ_x). For a low β insertion we have about 90° phase advance between the IP and the long-range collision region. Since in the LHC the betatron phase advance between long-range collisions on one side of the interaction region is very small, we can lump all n_{par} parasitic collisions into a single one, to reduce the computing time. This overestimates the effect slightly because the bunches oscillate with different phases with respect to each other.

Because a static dipole kick would change the closed orbit of the bunch, the static kick from the long-range collision must be subtracted [12]. The beam-beam long-range kick used in our simulation code is then

$$\Delta v_x(n) =$$

$$n_{par} \frac{2 r_p N_p^*}{\gamma} (E_x(x + L_x\sigma_x, y) - D_x(L_x\sigma_x, 0)). \quad (3)$$

where $D_x(L_x\sigma_x, 0)) = -1/L_x\sigma_x(1.0 - \exp(-\frac{L_x^2}{2.0}))$ is the (constant) dipole kick generated by a Gaussian distribution at a distance $x = L_x\sigma_x$. This assumes that a closed orbit exists [11] and the bunches oscillate coherently around this orbit. At the LHC, there are about $n_{par} = 16$ parasitic encounters on each side of an IP, with a minimum transverse separation of $L_x = 7.5$ (in units of σ_x). The fractional part of the horizontal and vertical tunes are 0.31 and 0.32, and unlike LEP [13], the results are not strongly affected by dynamic beta effects. In Figs.1 and 2 we show comparisons between the beam-beam kicks calculated with the HFMM and those obtained from an analytical expression, both for the case of round, exactly Gaussian beams.

In the Fig.1 we test the different methods for the charge assignment for a grid spacing of 0.25σ with a grid of 81x81, where 81 is the number of grid points in each plane. Thus the grid for the head-on collisions covers the amplitudes between -10σ to $+10\sigma$. While the 'nearest-grid-point' assignment gives visibly discontinuous values, the force evaluated with the CIC assignment is continuous and therefore preferable.

In the Fig.2 we have used a different grid spacing of 0.10σ with a grid of 201x201 to test the obtained accuracy. The effect of the discontinuous values in the 'nearest-grid-point' assignment is now smaller and barely visible as one could expect. The grid size for the simulation is a compromise between precision and computing speed. A grid spacing of 0.1 σ or below gives good results. For most simulations we have therefore chosen such a spacing and the Cloud-in-Cell (CIC) charge assignment.

5 SIMULATION RESULTS

In this section we shall give quantitative results on the coherent modes for head-on as well as some first results with long-range interactions. Since the symmetry of beam parameters plays an important role for the coherent motion, we study the relevance of intensity differences as well as tune and beam size asymmetries. They are expected to make it more difficult to maintain a coherent motion and will eventually help to avoid it.

5.1 Head-on collisions with equal betatron tunes and intensity

First let us consider the strong-strong case and head-on collisions of two round bunches, using the previous maps. The statistical variation in the initial distribution of particles is sufficiently large to excite the coherent modes. We start with equally strong beams, i.e. the intensity ratio R_I between the weaker and stronger beam is 1.0. If we perform a harmonic analysis of the motion of the barycentre of one bunch, we find two coherent modes. One is located at the unperturbed tune Q, the other has a lower frequency. In Fig. 3 we plot the amplitude frequency spectrum. The horizontal axis gives the tune shift from the unperturbed tune Q in units of ξ (i.e.: $w = \frac{\nu - Q}{\xi}$, for the round beam case $\xi_x = \xi_y = \xi = 0.0034$, $Q_x = 0.31$, $Q_y = 0.32$). For the other beam and the other plane a similar picture is obtained. Analysing the spectra of the distance between the centroids, i.e. the expressions $< x^{(1)} > - < x^{(2)} >$ and $< y^{(1)} > - < y^{(2)} >$, the coherent mode at the unperturbed frequency disappears. On the other hand, when we analyse the sum of the centroids ($< x^{(1)} > + < x^{(2)} >$, $< y^{(1)} > + < y^{(2)} >$) the lower mode frequency disappears. We can thus identify the mode at the unperturbed frequency as the so-called σ-mode, for which the centroids of the bunches oscillate in phase with equal frequencies and amplitudes. The lower frequency mode is called π-mode and in this mode the centroids oscillate also with equal frequencies and amplitudes but in opposite phase. The motion of the bunch centroids is a superposition of these two modes.

Between the π- and the σ-mode in Fig. 3 we find the incoherent *continuum*. A single particle crossing the opposing beam at a distance from its axis feels a defocusing force (or focusing force in the case of oppositely charged beams like LEP), which leads to a change in its tune. For particles near the centre of the counter rotating beam this tune shift is equal to $-\xi$. For particles further away the defocusing force is smaller (due to the non-linearity of the beam-beam force) and vanishes asymptotically. This creates an incoherent tune spread which extends from 0 to $-\xi$.

In our simulations we find the π-mode at a tune shift of exactly 1.21 ± 0.005 in units of ξ (and $\xi = 0.0034$). The π-mode is thus shifted outside of the continuum. The shift calculated with HFMM is therefore in excellent agreement with the theoretical prediction [1, 4].

5.2 Head-on collisions with equal betatron tunes and different intensity

It has been predicted [4] that for intensity ratios of 0.6 or lower, the π-mode merges with the continuum. In the soft Gaussian model this prediction cannot be tested exactly since the π-mode tune shift is underestimated [2, 3]. In this section we can now make a more precise quantitative comparison. Fig. 4 clearly confirms this prediction: the π-mode merges into the incoherent spectrum at Alexahin's ratio of 0.6 and is Landau damped. In the LHC the expected bunch to bunch intensity difference may be as large as $\pm$ 20%. Although this alone will not be sufficient to recover Landau damping, together with other uncertainties (see e.g. section 5.4) and suggested remedies (see next section) it should simplify the damping of the modes.

5.3 Head-on collisions with different betatron tunes

The first proposed remedy to avoid coherent beam-beam modes was to decouple the two beams by using different fractional tunes for their tunes [14]. This is possible in the LHC since we have two separate rings. Possible unwanted side effects of such a scheme were discussed in [15]. The sensitivity to the expected small tune differences is demonstrated here quantitatively. While the fractional part of beam 1 is kept at 0.310, the tune of the second beam is slightly varied. For a tune difference between the two beams of more than approximately $\approx$ $0.7\ \xi$ the π-mode disappears into the continuum as shown in Fig.5.

5.4 Head-on collisions with different beam sizes

Similar to an intensity imbalance, different beam sizes of the two beams can lead to loss of coherence and damped coherent modes. In Fig.6 we show the spectra for beam

size ratios of 0.90 and 0.70. Since the beam size (of the second beam) is now smaller, the tune shift is slightly larger than in the original case. While for a ratio of 0.90 the π-mode is still very visible, it has merged with the incoherent spectrum for 0.70. The mechanism is the same as for a beam intensity imbalance. At this point one can speculate whether the size imbalance can be compensated by an intensity imbalance, adjusted to give the same beam-beam tune shift parameter ξ. The result of such a simulation is shown in Fig.7 with the beam radius of the second beam reduced to 0.7, but with a smaller beam intensity (50%). The beam-beam parameter is therefore the same. We observe a clear coherent mode again. This observation however is non trivial. When the beams have different sizes and geometrical distributions, the fields seen by the two beams are rather different, although the tune shift parameter for the small amplitude particles is the same. The reason is that the larger beam experiences a very non-linear force for particles at much smaller amplitudes than the smaller beam. Particles at larger amplitudes must therefore behave rather differently. For the single particle behaviour, i.e. population of beam tails and lifetime, this is known to be of extreme importance [16, 17]. For a coherent oscillation it is mainly the oscillation frequency that must be the same and it is known that for the head-on collisions studied in this example, it is mainly the core of the beam contributing to the coherent oscillation and the tune shift. The core particles experience always an almost linear force proportional to the beam-beam parameter and this explains the observation.

Similar observations have been made in simulations of asymmetric colliders such as PEP-II [18] where the energy transparency condition was studied, i.e. where the energy asymmetry was compensated by an asymmetry of the beam currents.

5.5 Coherent modes from long-range collisions

Since the transverse distance between two bunches at the parasitic collision is larger than the rms beam size, the effects will be similar to the coherent interaction of rigid, point-like bunches. In that case the contribution of parasitic crossings to the tune shift of coherent oscillation modes would be

$$\begin{aligned} \Delta\nu_\pi &= 2 \times \text{(incoherent long-range tune shift)} \propto 1/L_x^2 \\ \Delta\nu_\sigma &= 0. \end{aligned}$$

Moreover, the incoherent long-range tune shifts for beam separations larger than $\approx 1.5\,\sigma$ have different signs for the two planes. Both, the coherent and incoherent tune shifts depend on the separation and for sufficiently large separation they scale with the inverse of the separation squared.

Most important however, the width of the incoherent spectrum (tune spread) of long-range collisions alone depends on the separation and in the LHC is smaller than the tune spread from head-on collisions [19, 20]. The distance of the π-mode from the edge of the incoherent spectrum is therefore rather different from the head-on case and one must expect a different behaviour. In particular the necessary measures to merge the coherent modes with the incoherent spectrum must be at least quantitatively different. In this report we have a first look at the dynamics of long-range collisions separately to demonstrate the differences. For an evaluation of the necessary operational parameters, both head-on as well as long-range collisions must be considered together, like it was done with the Gaussian approximation [2]. A more complete study should also include multiple bunches and interaction points and will be treated at a later stage [21].

5.6 Simulation of long-range collisions

The simulation of coherent modes from separated beams is a good example where the HFMM can be used to great advantage. In a conventional particle-mesh method, most grid points between and around the beams are empty and with a typical separation around 10 σ the necessary computing time becomes unacceptable. With the HFMM we have the option to either treat the opposing beam as a halo or to choose the grid large enough to cover both beams. Although at first sight the second option looks like a conventional grid method, the advantage is clear: the fields are calculated with the FMM field solver only at the grid points with charges and the saving in computing time is large. Treating the opposing beam as a real halo object usually requires more time than covering the whole area. In Fig.8 we show the horizontal spectrum for long-range collisions with a horizontal separation $L_x = 10.0$ (in units of σ_x). We plot it again as a function of the distance to the unperturbed tune, normalized to the head-on beam-beam tuneshift ξ, to allow a quantitative comparison to the head-on modes. For one of the figures (left) the particles in the opposing beam were treated as halo particles, i.e. were not covered by the grid. In the right figure the grid was extended to 15σ, i.e. included both beams. Both methods give the same results, however the computing speed is very different. The treatment as real halo is very time consuming. The real difference to a particle-mesh code then comes from the fact that only grid points with particles are treated, thus the number of computations scales like $O(N_p)$. The computing speed difference is about a factor 2.5 between the two options, therefore in all simulations we choose the procedure to cover the whole area with a grid, including both beams.

Like in the case of head-on coherent modes we identify the σ- and π-mode easily by analysing the sum and the difference of the barycentres separately. The peaked structure between the two modes represents again the incoherent continuum, this time arising from the long-range interaction. As expected, the coherent shift is two times larger than the shift of the incoherent spectrum.

5.7 Long range collisions with equal tunes

Fig. 9 shows the horizontal and vertical spectra of centroid oscillations of a bunch subject to long-range collisions with a horizontal separation of $L_x = 10.0\sigma_x$. To obtain realistic tune shifts, we have lumped all 32 long range interactions of a LHC interaction region into a single collision. The optics and geometry of the interaction regions permits this simplification [2, 12]. The horizontal axis gives the tune shift relative to the unperturbed tune Q in units of the head-on beam-beam parameter ξ: $w = \frac{\nu - Q}{\xi}$. In the horizontal plane, the tune shifts are positive, and the coherent dipole π-mode has twice the incoherent tune shift. In the vertical plane, the tune shifts are negative. The normalized tune shifts of the π-modes are $(w_x, w_y) = (0.645 \pm 0.005, -0.644 \pm 0.005)$. In Fig.10 we show the results for a separation of 6.0 σ_x and find values of $(w_x, w_y) = (1.828 \pm 0.005, -1.762 \pm 0.005)$. Comparing Figs. 9 and 10, the larger tune shift for the smaller separation is clearly visible as well as the increased tune spread of the incoherent spectrum. Both scale with $1/L_x^2$ as expected.

6 CONCLUSIONS.

We have implemented the HFMM technique to describe the beam-beam collision of two beams in the strong-strong regime. This allows us to study, by means of multi-particle tracking and with no approximation in the evaluation of the electromagnetic force, the coherent modes of oscillations of two colliding beams. Future improvements shall extend this work to several bunches per beam and, in particular, will allow us for the first time to study details of the modes excited by long-range interactions.

7 ACKNOWLEDGEMENTS

We should like to express our gratitude to M. Craddock (TRIUMF) for supporting this study and to M. D'Yachkov (TRIUMF) who has first suggested the use of the Fast Multipole Method for our problem.

8 REFERENCES

[*] Present Address: BULL, Paseo Doce Estrellas 2, 28042 Madrid, SPAIN

[1] K. Yokoya, H. Koiso, *Tune shift of coherent beam-beam oscillations.* Particle Accelerators, Vol. **27**, 181 (1990).

[2] M.P. Zorzano, F. Zimmermann, *Coherent beam-beam oscillations at the LHC.* CERN, LHC Project Report 314, (1999).

[3] K. Yokoya, *Limitation of the Gaussian approximation in beam-beam simulations.* Phys.Rev.STAB, Vol. **3**, 124401 (2000).

[4] Y.I. Alexahin, *On the Landau damping and decoherence of transverse dipole oscillations in colliding beams.* Particle Accelerators, Vol. **59**, 43 (1999).

[5] Y.I. Alexahin, *A study of the Coherent Beam-beam Effect in the Framework of the Vlasov Perturbation Theory.* CERN, LHC Project Report 467, (2001).

[6] S. Krishnagopal and R. Siemann, *Coherent beam-beam interactions in electron-positron colliders.* Phys.Rev.Lett., Vol. **67**, 2461 (1991).

[7] L. Greengard, *The rapid evaluation of potential field in particle systems.* Thesis, Yale (1987),Cambridge, Mass. MIT Press, 1988.

[8] L. Greengard and V. Rokhlin, *A fast algorithm for particle simulations.* J.Comp.Phys. Vol. **73**, (1987).

[9] F.W. Jones, *A Hybrid Fast-Multipole Technique for Space-Charge Tracking With Halos.* In Proceedings of the workshop on Space Charge Physics in High Intensity Hadron Rings, Shelter Island NY, May 1998, (AIP Conf. Proc. 1998) 448.

[10] F.W. Jones, *Development of the ACCSIM tracking and simulation code.* In Proceedings of the 1997 Part. Acc. Conf. Vancouver, May, 1997.

[11] H. Grote, *Self-consistent orbits with beam-beam effect in the LHC.* CERN, LHC Project Report 404, (2000).

[12] W. Herr, *Coherent dipole oscillations and orbit effects induced by long-range beam-beam interactions in the LHC.* CERN/SL/91-34 (AP) (1991).

[13] D. Brandt, W. Herr, M. Meddahi, A. Verdier. *Is LEP beam-beam limited at its highest energy?.* In Proceedings of the 1999 Part. Acc. Conf., New York 1999, (1999).

[14] A. Hofmann, *Beam-beam modes for two beams with unequal tunes.* In Proceedings of the LHC-99 Beam-beam workshop at CERN, 1999, edited by J. Poole and F. Zimmermann (CERN, Geneva, 1999).

[15] Y.I. Alexahin and M. P. Zorzano, *Excitation of Coherent Beam-Beam resonances for beams with unequal tunes in the LHC.* CERN LHC Project Note 226, 2000 (unpublished).

[16] M. Meddahi, *Effets faisceau-faisceau dans le collisionneur protons-antiprotons du SPS.* PhD Thesis, Univ. Paris 7 and CERN SL 91-30 (BI) (1991).

[17] L. Evans, J. Gareyte, M. Meddahi, R. Schmidt, *Beam-beam effects in the strong-strong regime at the CERN-SPS.* In Proceedings of 1989 Part. Acc. Conf., Chicago 1989, (1989).

[18] S. Krishnagopal, *Energy transparency and symmetries in the beam-beam interaction.* Phys.Rev.STAB, Vol. **3**, 024401 (2000).

[19] W. Herr and J. Miles, *A comparative study of beam-beam tune footprints for colliding beams with a crossing angle and offset vertex in LHC V4.1.* CERN LHC Project Note 4, 1995 (unpublished).

[20] O. Meincke and H. Grote, *Tune footprints for collision optics 5.0,* CERN LHC Project Note 161, 1998 (unpublished).

[21] W. Herr, M.P. Zorzano and F. Jones, *Analysis of coherent long-range interactions using a Hybrid Fast Multipole Method.* To be published.

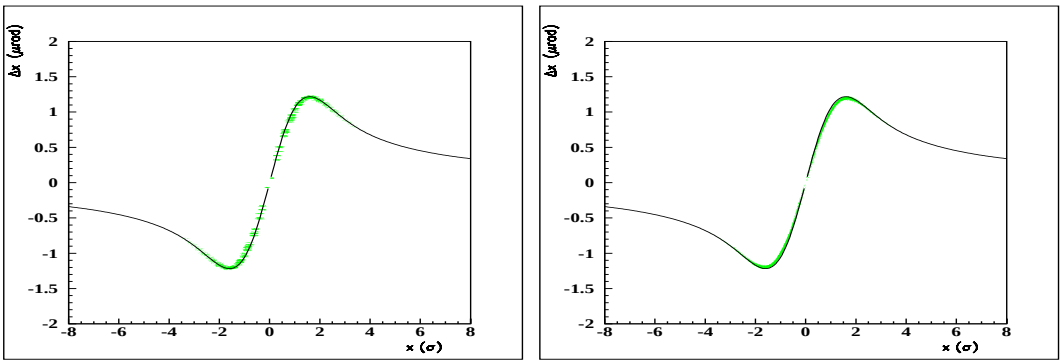

Figure 1: Beam-beam kick as calculated with HFMM (points) and from analytical expression (solid line) for round beams with Gaussian distribution. Left figure with 0.25σ grid (81x81) and 'nearest-grid-point' assignment. Right figure with 'cloud-in cell' (CIC) assignment.

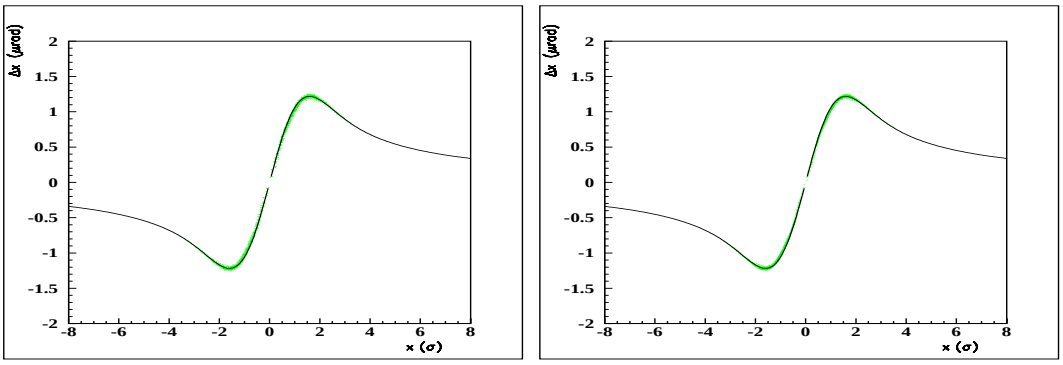

Figure 2: Beam-beam kick as calculated with HFMM (points) and from analytical expression (solid line) for round beams with Gaussian distribution. Left figure with 0.10σ grid (201x201) and 'nearest-grid-point' assignment. Right figure with 'cloud-in cell' (CIC) assignment.

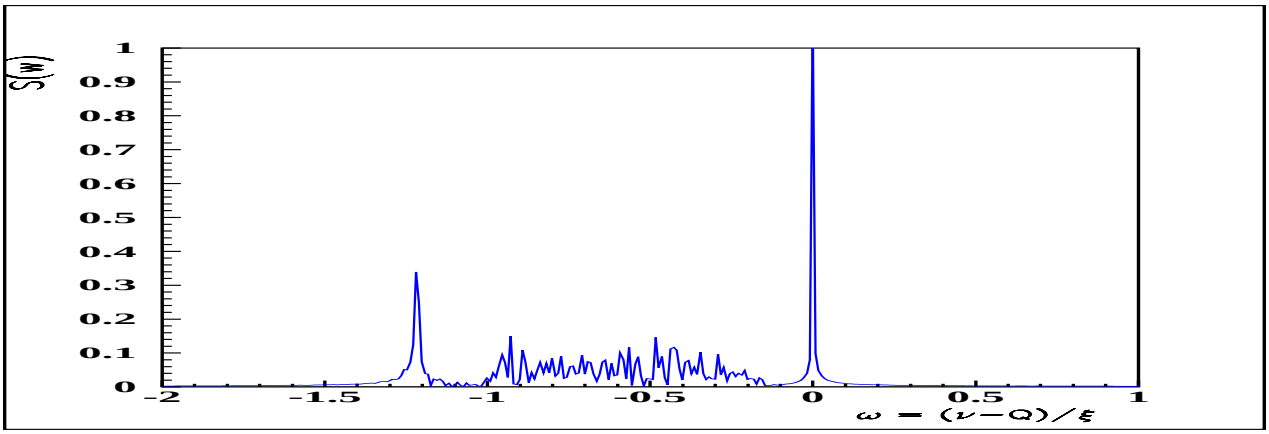

Figure 3: Frequency spectrum of the bunch centroid motion (for 2^{17} turns, $N = 10^4$ macroparticles) for round beams. The grid covers from -10σ to 10σ, the rest of the particles being treated as halo particles. The horizontal axis gives the tune shift from the unperturbed tune Q in units of ξ, *i.e.* $w = \frac{\nu - Q}{\xi}$. The vertical axis is the corresponding amplitude. The π- and σ- oscillation modes are clearly visible.

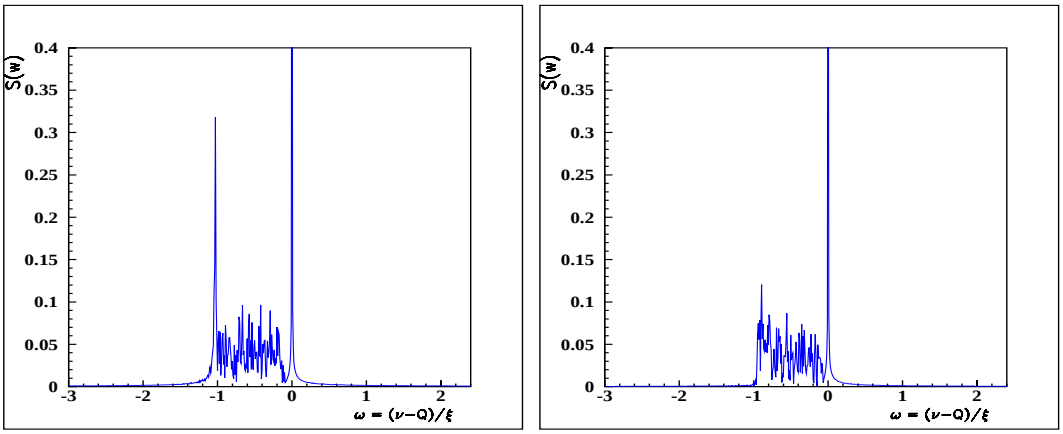

Figure 4: Frequency spectrum of the bunch centroid motion (over 2^{17} turns, $N = 10^4$ macroparticles) for round beams and intensity ratio R_I = 0.65 (left) and 0.55 (right).

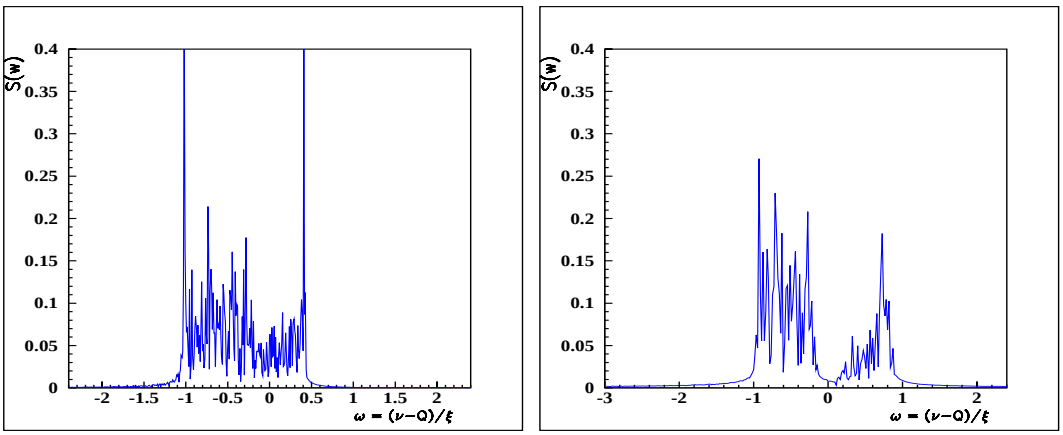

Figure 5: Frequency spectrum of the bunch centroid motion (for 2^{17} turns, $N = 10^4$ macroparticles) for round beams and different fractional tunes of the second beam: 0.312 (left) and 0.313 (right). The tune of the first beam is kept at 0.310.

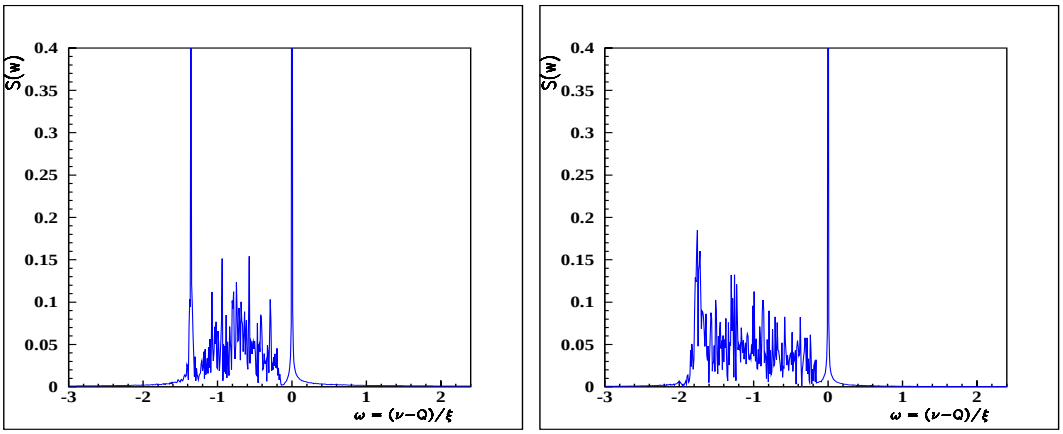

Figure 6: Frequency spectrum of the bunch centroid motion (for 2^{17} turns, $N = 10^4$ macroparticles) for round beams and size ratios $\sigma^{(2)}/\sigma^{(1)}$ of 0.90 (left) and 0.70 (right).

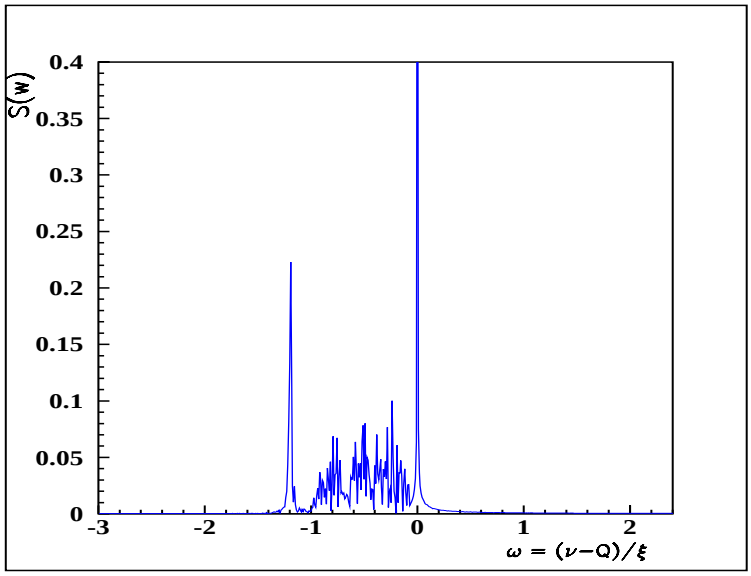

Figure 7: Frequency spectrum of the bunch centroid motion (for 2^{17} turns, $N = 10^4$ macroparticles) for round beams and size ratios $\sigma^{(2)}/\sigma^{(1)}$ = 0.70 and intensity ratio R_I = 0.5.

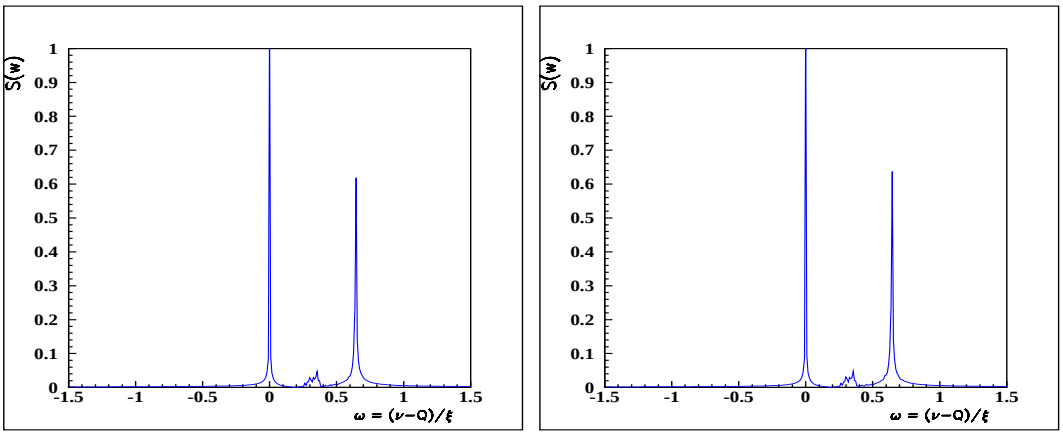

Figure 8: Spectrum of the horizontal centroid motion for long-range collisions with horizontal separation $L_x = 10.0$ (in units of σ_x) and no head-on collision (2^{15} turns, $N = 10^4$ macroparticles). For the left figure the grid did not cover both separated beams, i.e. the particles in the second beam were treated as halo particles. In the right figure the grid covered both beams.

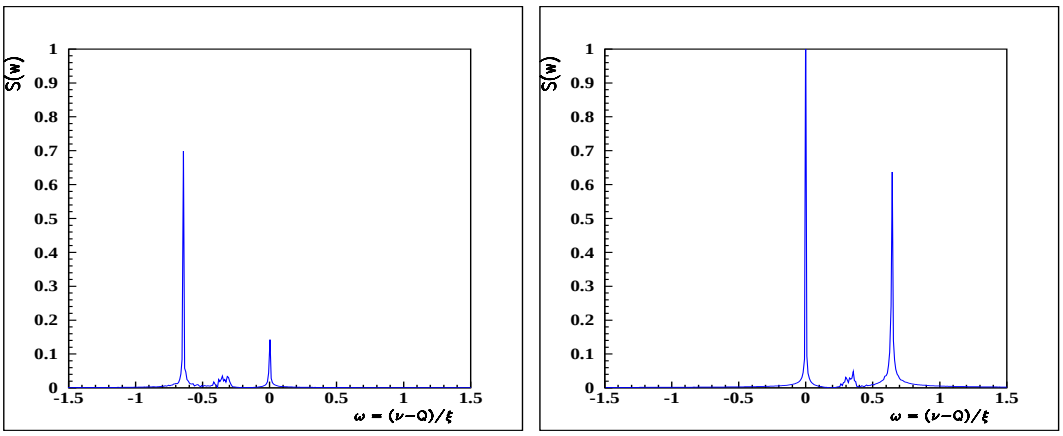

Figure 9: Spectrum of the vertical (left) and horizontal (right) centroid motion for long-range collisions with horizontal separation $L_x = 10.0$ (in units of σ_x) and no head-on collision (2^{15} turns, $N = 10^4$ macroparticles). The tune shifts due to long-range collisions have opposite sign in the two transverse planes. The coherent π-mode is at twice the incoherent tune shift.

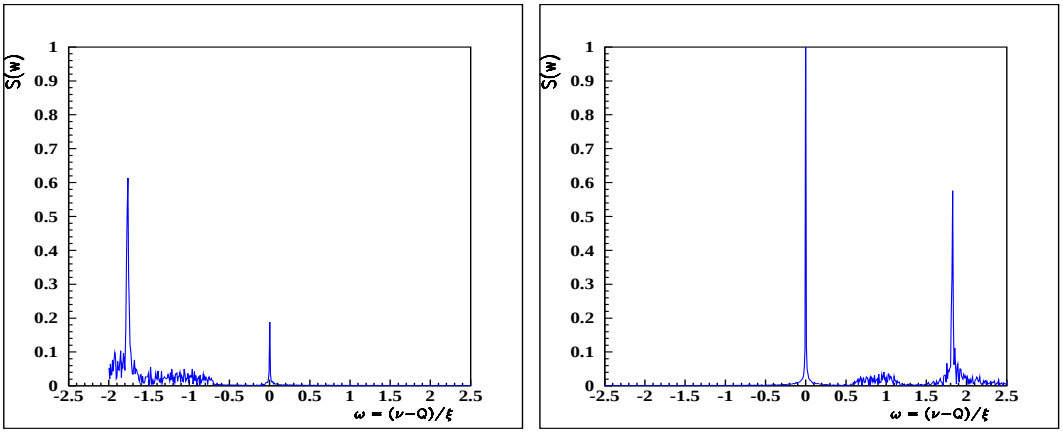

Figure 10: Spectrum of the vertical (left) and horizontal (right) centroid motion for long-range collision with horizontal separation $L_x = 6.0$ (in units of σ_x) and no head-on collision (2^{15} turns, $N = 10^4$ macroparticles). The tune shifts due to long-range collisions have opposite sign in the two transverse planes.

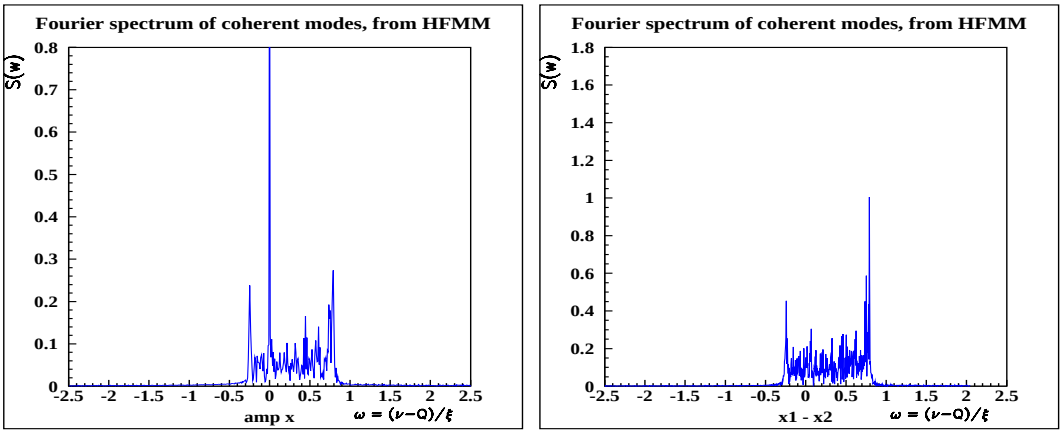

Figure 11: Spectrum of the horizontal centroid motion for head-on together with long-range collision with horizontal separation $L_x = 6.0$ (in units of σ_x) 2^{15} turns, $N = 10^4$ macroparticles. planes. In the right figure π-oscillations only.

Weak–Strong Beam–Beam Tracking for LHC V6.0

Y. Luo and F. Schmidt, CERN, Geneva, Switzerland

Abstract

Simulations have been performed for the LHC for a complete model of the LHC with the multipole errors of all dipoles and quadrupoles and the triplet errors, at injection and collision energy respectively. For the two energies the weak–strong beam–beam forces are included in the simulations for both the head–on and the long–range collisions by using a realistic beam separation scheme. The transverse amplitudes have been densely varied and several phase space angles have been treated. It has been found that the typical tracking periods of 10^5 turns are not sufficient but that the tracking has to be extended to at least 10^6 turns. We will demonstrate that early indicators can help to find not too pessimistic bounds for long–term stability.

1 INTRODUCTION

The LHC model studied in this note is based on LHC version 6.0, with ATLAS, CMS, LHCB head–on collisions and ALICE halo collisions. The lattice is anti–symmetric about all four IPs. At injection energy the errors of the main dipole's of error table 9901 (see for instance Ref. [1]) are considered together with the b3 and b5 spool piece correction system. At top energy the errors of low–beta triplet quadrupoles (details see below) are introduced counteracted by two types of correction packages with b_3, b_6 and b_4, a_3, a_4 correctors respectively. The beam–beam interaction was simulated in the weak–strong approximation. The dynamic aperture (DA) is defined as the maximum radius for which the particles are stable for 10^5 or 10^6 turns. A series of tracking studies are performed for five different radial angles in the phase space. The phase space angle is defined as $\phi = \arctan\sqrt{\epsilon_y/\epsilon_x}$, in this paper the angles ϕ =15°, 30°, 45°, 60° and 75° have been used. To determine the minimum dynamic aperture to a confidence level of 95% the simulations have been performed for 60 different representations of the random components of the multipole errors (seeds). All tracking runs has been performed with the SixTrack code [2].

2 TRIPLET ERRORS AND THEIR CORRECTION

At top energy the field errors in the low–beta triplets play an important role in the reduction of the dynamic aperture. The largest components of the latest triplet errors are given in Table 1. The body and end effects have been combined into one single number for the thin–lens approach used here: each triplet quadrupole is split into four thin–lens quadrupoles at each of IP1, IP2, IP5, IP8.

Component		systematic	uncertainty	random
b3		0	0.72	0.36
b4		-0.175	0.83	0.36
b6		0.34	0.91	0.21
a3		0	0.69	0.34
a4		0	0.33	0.34
Component		systematic	uncertainty	random
b3		0	0.63	0.34
b4		0	0.22	0.34
b6		0.21	0.41	0.18
a3		0	0.32	0.34
a4		0	0.26	0.34

Table 1: *Low-beta quadrupole field errors for KEK version 4.x(upper) and FNAL version 3.1 (lower). Values are relative to the main field at* $x = 17mm$ *in units of* 10^{-4}.

On either side of IP1, IP2, IP5, and IP8 two corrector groups are placed as proposed by J. Strait at a CERN–KEK–US meeting, April 2000. Each corrector group contains several correction spools such that on either side of each IP one corrector exists for b3, b4, b6, a3 and a4. The correction formalism follows the one outlined by A. Verdier and A. Faus–Golfe [3]. The principle is rather simple: with one corrector for each multipole component on either side of each IP, we compensate the total kick for purely horizontal and purely vertical motion simultaneously.

3 BEAM SEPARATION SCHEME

There are 15 parasitic crossing points on either side of each IP. The total crossing angle at collision is fixed throughout to 300μrad. The crossing is horizontal in IP5 and IP8, while at IP1 and IP2 it is vertical [4]. The bunch sizes in the opposite beam appearing in the beam–beam element were calculated under the assumption of full anti–symmetry at all four IPs; the beam separation was taken as the distance of the orbits in ring 1 and ring2. The beam–beam separation in injection and collision mode are shown in

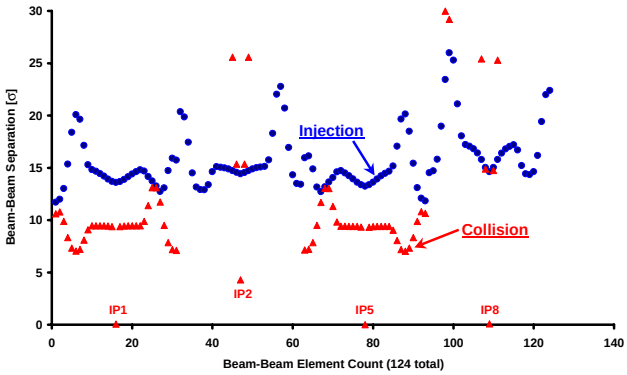

Figure 1: *LHC 6.0 beam–beam separations at the four IPs, (blue) circles for the injection and (red) triangles for the collision case respectively.*

Figure 1, where the separations at injection and collision are given in the units of beam size in the corresponding crossing plane, the horizontal axis is the count number of the beam–beam encounters, 124 in total, around the four IPs. At collision energy the separation is about 9.5 σ while at injection energy it varies between 12 and 15 σ.

4 DYNAMIC APERTURE IN COLLISION WITHOUT BEAM–BEAM

First the correction scheme of the low–beta triplet errors has been investigated with the LHC collision mode without beam–beam interaction. Figure 2 shows the dynamic apertures of 10^5 turn tracking before and after triplet error corrections.

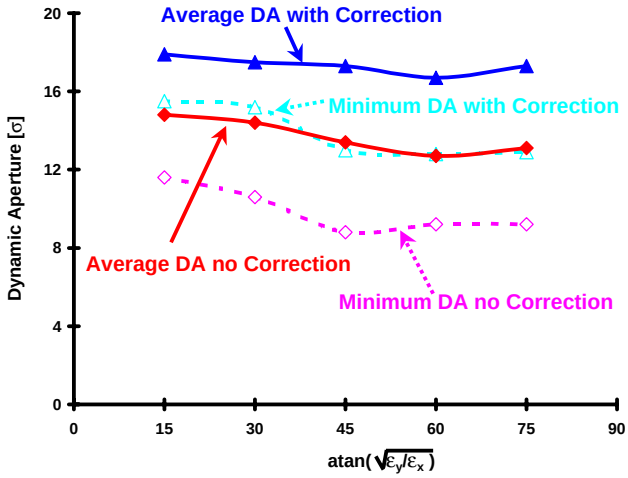

Figure 2: *Dynamic aperture without and with low–beta triplet field error correction. The beam–beam kicks are not included and the tracking has been performed for* 10^5 *turns.*

The triplet errors reduce the average and minimum dynamic aperture to about 13 σ and 9 σ respectively for 10^5 turns. This is mainly due to the large b_6 component of the quadrupoles. After correction, as described above, the average and minimum dynamic apertures increase to some 17 σ and 13 σ respectively, i.e. a gain of about 4 σ. So we conclude that the proposed triplet error correction scheme is indeed very effective. It has to be mentioned that only part of this improvement of the DA remains in the presence of the parasitic beam–beam kicks (see Ref. [5]).

5 DYNAMIC APERTURE AT COLLISION INCLUDING BEAM–BEAM

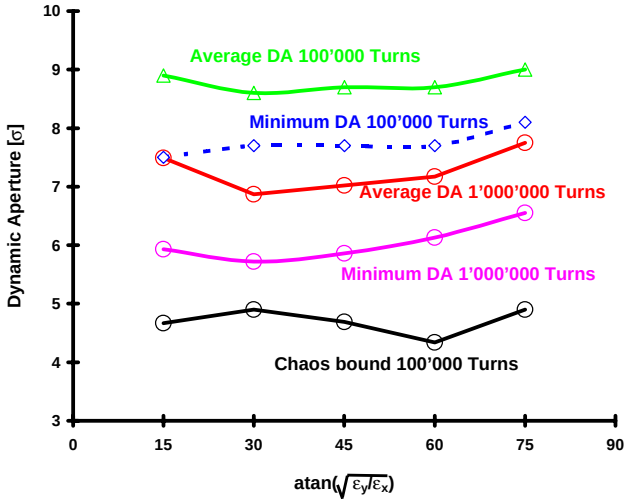

Figure 3: *Dynamic aperture at collision including beam–beam kicks. Tracking is performed for* 10^5 *and* 10^6 *turns.*

Figure 3 shows the results for 10^5 and 10^6 turns when the beam–beam interaction is included. Tracking for 10^5 turns shows the average DA to go down to about 9 σ, while the minimum DA is 7.5 σ. As found earlier [6, 7] this reduction is due to the many parasitic beam–beam crossings. We know from numerous tests that the DA for plain nonlinearities is not decreasing very much for tracking runs in excess of 10^5 turns (see Ref. [8]). It was therefore surprising that there is a dramatic decrease of the DA when the tracking is extended to 10^6 turns. The average and minimum DA becomes about 7 and below 6 σ respectively. Our conjecture for this large reduction of the DA is the following: the above mentioned parasitic crossings make the motion very slightly chaotic at small amplitudes. As a result it takes considerable time until a particle is driven to large enough amplitudes such that the nonlinearities are strong enough to cause the loss of the particle. In fact, the chaotic bound (see below) goes down to about 4 σ and it has to be feared that particle loss may take place down to that level when the tracking is extended beyond 10^6 turns. Presently, our computer power is insufficient to allow systematic studies with those large turn numbers.

6 DYNAMIC APERTURE AT INJECTION WITHOUT AND INCLUDING BEAM–BEAM

Tracking including beam–beam over 10^5 turns at injection energy (Figure 4) gives about 10 σ for the minimum DA which is more than 1 σ smaller than without the beam–beam kicks. Also in this case there is a sizable reduction of the DA when the tracking is extended to 10^6 turns, in particular at the phase space angle of 45°. In fact, the DA at that phase space angle agrees well with the chaotic bound which is found to have its minimum at about 7 σ.

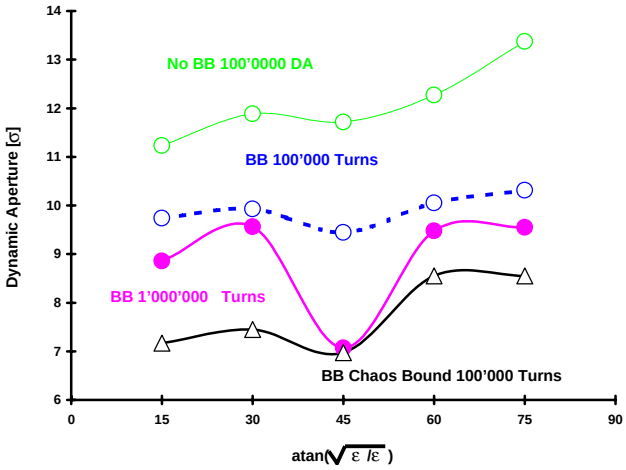

Figure 4: *Minimum dynamic aperture at injection without and including beam–beam kicks. Tracking is performed for* 10^5 *and* 10^6 *turns.*

7 TUNE FOOTPRINTS FOR COLLISION AND INJECTION

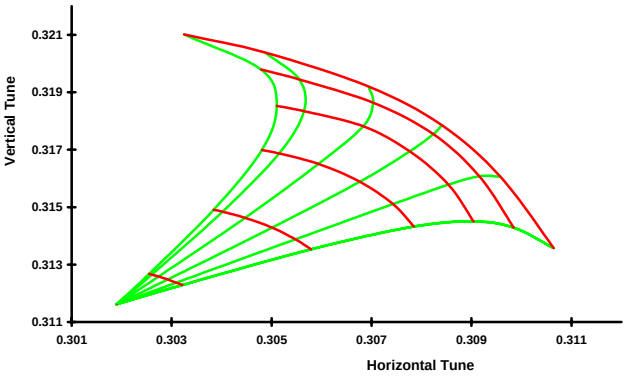

Figure 5: *Tune footprint at collision energy*

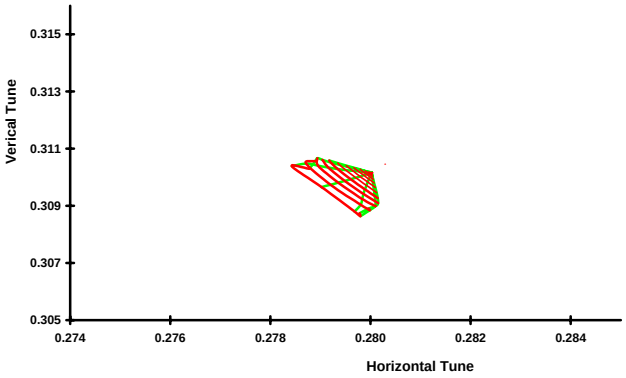

Figure 6: *Tune footprint at injection energy*

The tune footprints at collision and at injection are shown in Figure 5 and Figure 6 respectively. At injection energy one would naively expect that the beam–beam force will not deteriorate the DA by much since the tune footprint is so much smaller at that energy (the beams do not suffer from head–on collisions). Furthermore, this was to be expected since the beam separation is so much larger at injection. However, as we have seen in the last section, the DA has been reduced by a considerable amount and at one phase space angle by as much as 4 σ. From this we have to conclude that the parasitic beam–beam kicks are relevant with respect to the DA even for separation in excess of 12 σ.

8 EARLY INDICATOR OF PARTICLE LOSS

Since many years the onset of chaos was used as an early indicator of particle losses (for a more complete review see Ref. [9]). However, due to the fact that the dynamic aperture does not reduce much beyond 10^5 turns, the indicator rendered too pessimistic estimates of the DA. However, this is obviously no longer true when beam–beam kicks have been introduced in the simulations. It seems therefore worthwhile to reexamine this technique. The first observation has been that the global onset of chaotic motion is too optimistic. Instead, one has to watch for nests of chaotic motion, which we call “chaotic spikes”, inside the mostly regular regime, i.e. at smaller amplitudes. Of course, by definition, there always exist very thin chaotic regimes deep in the regular domain which will not lead to particle loss after finite times. Our pragmatic approach is to choose a certain width of the chaotic spike as a criterion for very long–term losses. For this report we have chosen a spike width of some 0.3 σ, but this has to be further optimised to render reliable results.

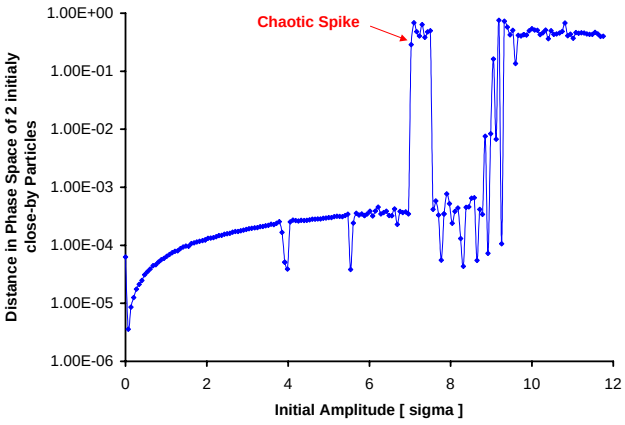

Figure 7: *Example for a chaotic spike. A chaotic spike we consider a limited range of amplitudes with chaotic behaviour. This has to be distinguished from the broad onset of chaos where particle loss sets in rather quickly.*

Chaos is typically being detected by following the evolution of the distance of phase space of two initially close–by particles. Figure 7 shows an example of such a distance after 10^5 turns. Whenever this distance rises by many orders of magnitude (the maximum is normalised to 1) the motion exhibits chaotic behaviour. The (red) arrow in the figure indicates what we call a chaotic spike and the probable long–term DA.

In Figure 8 this techniques is shown in action for the 300 individual tracking runs that make a typical study case (60 seeds and 5 phase space angles): the upper curve, (red) squares, shows the 10^5 turns DA, the medium curves, (blue) triangles, depicts the 10^6 turns DA and lastly the lower curve, (magenta) diamonds, demonstrates that chaotic spikes derived from 10^5 turns can serve as a not too pessimistic indicator of long–term losses.

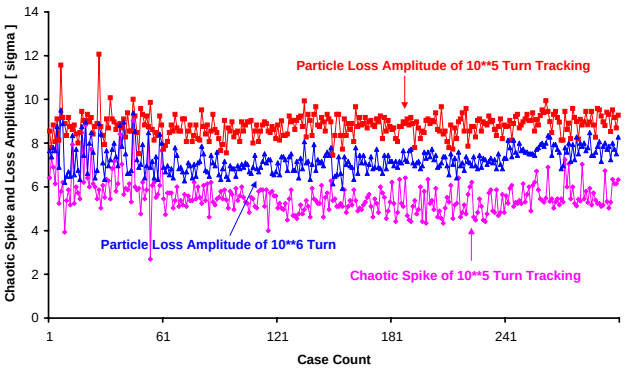

Figure 8: *DA for 10^5 turns (upper curve (red) squares) and 10^6 turns (medium curve (blue) triangles) in comparison with the chaotic spikes (lower curve (magenta) diamonds)*

9 AMPLITUDE BLOW–UP

Another interesting indicator of particle loss is the onset of the amplitude blow–up of a particle. In Figure 9 an example is shown with the maximum and mean amplitudes versus the initial amplitude. (The line "slope=1" represents the condition of mean amplitude equal to the initial one.)

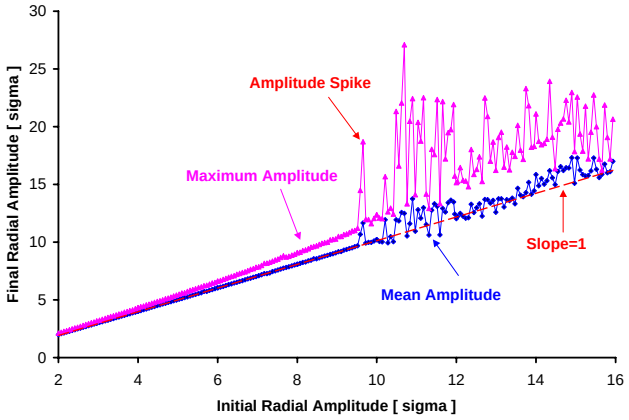

Figure 9: *Example for an amplitude spike.*

As for the case of the global onset of chaos the global amplitude blow–up is too optimistic to predict the long–term DA. As a criterion we define here the "amplitude spike" as that initial amplitude at which the maximum amplitude exceeds by 10% what is expected from previous maximum amplitudes.

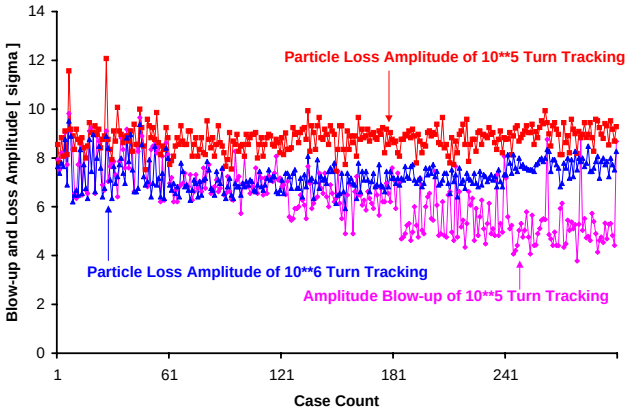

Figure 10: *DA for 10^5 turns (upper curve (red) squares) and 10^6 turns (medium curve (blue) triangles) in comparison with the amplitude spikes (lower curve (magenta) diamonds); compare with Figure 8.*

Figure 10 shows the same 10^5 and 10^6 turn DA curves as in Figure 8 but this time together with the amplitude spikes. This type of indicator also seems to have some predictive power but it is probable less reliable than the "chaotic spike" approach.

10 CONCLUSIONS

The DA of the LHC including beam–beam kicks has been studied for both injection and collision energy. In both cases the parasitic beam–beam kicks lead to sizable reductions of the DA. In particular, we observe that there are very slow but considerable losses at small amplitudes, such that our usual 10^5 turn tracking is by far to optimistic. By the same token early indicator become again important, since they allow to find only slightly pessimistic predictions of the DA for 10^6 turns and more.

11 ACKNOWLEDGEMENT

We would like to thank Hans Grote for providing us with the triplet correction settings and the beam separation at the locations of the beam encounters.

12 REFERENCES

[1] L. Jin and F. Schmidt, "Tune Scan Studies for the LHC at Injection Energy", LHC Project Report 377, http://wwwslap.cern.ch/frs/report/tune_scan99_v6.ps.gz.

[2] F. Schmidt, "SixTrack, Version 1, Single particle tracking code treating transverse motion with synchrotron oscillations in a symplectic manner", CERN/SL/90–11(AP) (1990).

[3] A. Verdier and A. Faus–Golfe, *Multipole Compensation in the LHC low–β Insertions*, PAC97 Vancouver, Conference Proceedings, and LHC Project Report 116.

[4] H. Grote, *Self-consistent Orbits for Beam-beam Interactions in the LHC*, LHC Project Note 216.

[5] L.H.A. Leunissen, H. Grote, F. Schmidt, "LHC Dynamic Aperture including the Beam-Beam Force", CERN–LHC–Project–Report–405, paper presented at the EPAC Conference in Vienna 2000, http://wwwslap.cern.ch/frs/report/TUP6B12.ps.gz.

[6] Y. Papaphilippou and F. Zimmermann, "Weak–strong beam–beam simulations for the LHC", Proceedings of the workshop on: "Beam–Beam Effects in Large Hadron Colliders –LHC99–", pp. 76–80, CERN–SL–99–039 AP, http://wwwslap.cern.ch/frs/report/workshop2_new.ps.gz.

[7] H. Grote, L.H.A. Leunissen and F. Schmidt, "LHC Dynamic Aperture at Collision", LHC Project Note 197, http://wwwslap.cern.ch/frs/report/lhcnotexx.ps.gz.

[8] M. Böge and F. Schmidt, "Estimates for Long–Term Stability for the LHC", LHC Project Report 114, presented in part at the Particle Accelerator Conference, Vancouver, 12–16 May, (1997), AIP Conference Proceedings 405 (1996), http://wwwslap.cern.ch/frs/report/conj97lhc.ps.gz, and contribution to the workshop on "New Ideas for Particle Accelerators", Santa Barbara, November 1996.

[9] F. Schmidt, F. Willeke and F. Zimmermann, "Comparison of methods to determine long–term stability in proton storage rings", CERN SL/91–14 (AP), DESY HERA 91–07, Part. Accel. **35**, pp. 249–256 (1991), http://wwwslap.cern.ch/frs/report/lyasl.ps.gz.

Weak-Strong Simulation Studies for the LHC Long-Range Beam-Beam Compensation

F. Zimmermann, CERN, Geneva, Switzerland

Abstract

Using weak-strong computer simulations, we study the improvement of LHC tune footprints and dynamic aperture by electromagnetic lenses, *i.e.*, pulsed wires, which compensate for the long-range beam-beam interaction. In particular, we explore the robustness of this compensation scheme to linear optics imperfections as well as to errors in wire strength and position.

1 INTRODUCTION

The long-range or parasitic collisions are expected to limit the dynamic aperture of the LHC [1, 2, 3]. A compensation scheme for the effect of the long-range collisions, proposed by J.-P. Koutchouk, is presently under investigation at CERN [4, 5, 6]. The compensation employs an electric wire on each side of each interaction point (IP). The wire carries an integrated current of about 80 Ampere meter, and it is placed at a horizontal or vertical distance from the beam that equals the effective beam-beam separation at the long-range encounters, about 9.5σ at top energy. If the current is pulsed or ramped at the start of each bunch train the correction can work even for the so-called PACMAN bunches [7], *i.e.*, for bunches which do not experience the full set of long-range encounters, due to gaps in the opposing beam.

In this report, we report weak-strong simulation results for the wire compensation scheme. The simulation program is the same as described in Ref. [2], except that two electric wires have been added. Considering two head-on collisions with alternating crossing and the parasitic collisions around each head-on IP, the simulation yields the tune footprints and the action diffusion rate at various betatron amplitudes. Using this simulation, we study the sensitivity of the wire compensation to various errors, such as to errors in the wire position, the wire strength, or the betatron phase advance between the wire and the collision point.

Section 2 describes the simulation model in more detail. Results are presented in Section 3. Conclusions are drawn in Section 4.

2 MODEL

The simulation study follows John Irwin's approach for the SSC [2, 8]. It is a 4-dimensional code, without synchrotron oscillations. However, tune modulation can be included as an option.

We consider two IPs, one with horizontal crossing, the other with vertical. This models the two main IPs in the LHC. Simulation parameters are summarized in Table 1. At the parasitic collision points the beams are separated by $\theta_c/\theta^*_{x,y} \approx 9.5$ rms beam sizes. The fractional tunes are set to the LHC design values of 0.31 and 0.32. The phase advance between IPs is taken to be exactly half the total phase advance per turn.

Table 1: Parameters.

parameter	symbol	value
number of particles per bunch	N_b	1.1×10^{11}
beam energy	E_b	7 TeV
rms beam size at IP	$\sigma^*_{x,y}$	16μm
rms divergence at IP	$\theta^*_{x,y}$	31.7 μrad
IP beta function	$\beta^*_{x,y}$	50 cm
full crossing angle	θ_c	300 μrad
number of main collision points	n_{IP}	2
parasitic collisions per side	$n_{\rm par}$	16
bunch spacing	L_{sep}	7.48 m
beam-beam parameter	ξ	0.00342
revolution frequency	f_{rev}	11.25 kHz

At each IP we apply a series of 3 kicks representing, respectively,

- the lumped effect of long-range collisions and wire compensation on the incoming side,
- a head-on collision,
- the lumped effect of long-range collisions and wire compensation on the outgoing side.

2.1 Head-On Collision

The head-on collision with a round Gaussian beam is parametrized as

$$\Delta x' = \frac{2r_p N_b}{\gamma}\,\frac{x}{r^2}\left(1-e^{-\frac{r^2}{2\sigma^{*\,2}}}\right) \qquad (1)$$

$$\Delta y' = \frac{2r_p N_b}{\gamma}\,\frac{y}{r^2}\left(1-e^{-\frac{r^2}{2\sigma^{*\,2}}}\right) \qquad (2)$$

where $\sigma^* \equiv \sigma_x = \sigma_y$; $r = \sqrt{x^2+y^2}$ is the radial distance to the origin, r_p the classical proton radius, γ the Lorentz factor, and N_b the bunch population. The phase-space coordinates x, x', y, and y' refer to the IP.

2.2 Long-Range Interactions

All parasitic collisions ($n_{\rm par}$) on one side of the IP are lumped into a single deflection. Assuming a perfect $\pi/2$

distance in phase advance between head-on and parasitic collision points, the kick is approximately expressed as a change in the IP coordinate (while the IP angle stays unchanged). For the IP with horizontal crossing, the IP coordinates and slopes are changed according to

$$\Delta x = n_{\rm par}\,\frac{2r_pN_b}{\gamma}\left[\frac{x'+\theta_c}{\theta_t^2}\left(1-e^{-\frac{\theta_t^2}{2\theta^{*2}}}\right) -\frac{1}{\theta_c}\left(1-e^{-\frac{\theta_c^2}{2\theta^{*2}}}\right)\right] \quad (3)$$

$$\Delta y = n_{\rm par}\,\frac{2r_pN_b}{\gamma}\,\frac{y'}{\theta_t^2}\left(1-e^{-\frac{\theta_t^2}{2\theta^{*2}}}\right) \quad (4)$$

where

$$\theta_t \equiv \left((x'+\theta_c)^2+y'^2\right)^{1/2} \quad (5)$$

and $\theta^* \equiv \theta_x^* = \theta_y^*$ is the rms IP beam divergence. At the LHC, the effective number of parasitic crossings per side is $n_{\rm par} \approx 16$. The expression for the kick is the same on both sides of the IP. The second IP, with vertical crossing, is treated analogously.

2.3 *Wire Compensation*

The new feature of the code is the electric wire. For a horizontal crossing, the effect of a thin wire is represented as:

$$\begin{aligned}\Delta x &= \frac{\mu_0 I_w l_w}{2\pi(B\rho)}\left[\frac{x'+\theta_{c,w}\pm\phi_x x/\beta_x^*}{\theta_{tw}^2}-\frac{1}{\theta_{c,w}}\right] \quad (6)\\ \Delta x' &= -(\pm 1)\phi_x\,\Delta x/\beta_x^*\\ \Delta y &= \frac{\mu_0 I_w l_w}{2\pi(B\rho)}\,\frac{y'\pm\phi_y y/\beta_y^*}{\theta_{tw}^2}\\ \Delta y' &= -(\pm 1)\phi_y\,\Delta y/\beta_y^*\end{aligned}$$

where

$$\theta_{tw} \equiv \left((x'+\theta_{c,w}\pm\phi_x x/\beta_x^*)^2+(y\pm\phi_y y/\beta_y^*)^2\right)^{1/2}, \quad (7)$$

and l_w is the length of the wire, $\theta_{c,w}$ is the angle at the IP representing the transverse distance between the beam and the wire, I_w the wire current, and $(B\rho)$ the magnetic rigidity of the beam. The $\pm$ signs refer to the two sides of the IP. Again the vertical crossing is treated in analogy. The errors ϕ_x and ϕ_y represent the deviation in phase advance from the IP with respect to the ideal value $\pi/2$. Simultanously they also give the differences in phase advance from the location of the long-range collisions. At the wire location presently contemplated, the phase errors are about 2–3° in the design optics [4]. For perfect compensation, the wire current must be chosen as

$$I_w = -4\pi(B\rho)N_b r_p n_{\rm par}/(\mu_0\gamma l_w). \quad (8)$$

The ideal distance between wire and beam is $d_w \approx (\theta_c/\theta_{x,y}^*)\sigma$, where σ denotes the rms beam size at the wire. This corresponds to $\theta_{c,w} = \theta_c$.

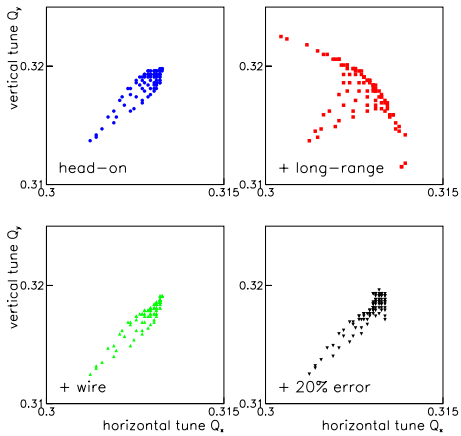

Figure 1: Tune footprints for various cases, for initial horizontal and vertical amplitudes extending to $7\sigma_{x,y}$. Top left: head-on collisions only; top right: head-on plus long-range collisions; bottom left: head-on plus long-range collisions and a perfect wire; bottom right: head-on plus long-range collisions and a wire with 20% strength error.

2.4 *Compensation Errors*

We consider five types of errors, namely,

- a simultaneous symmetric betatron phase error $\phi_{x,y}$ on both sides of each IP,
- a static wire strength error,
- a random wire strength error,
- a wire position error,
- a betatron phase error $\phi_{x,y}$ with only one wire per IP.

Simulation results for each case are discussed next.

3 RESULTS

Figure 1 shows tune footprints computed for initial amplitudes extending to $7\sigma_{x,y}$. The tunes were calculated by applying a fast Fourier transform to particle positions sampled over 4096 turns. The top left picture shows the tune footprint for the two head-on collisions alone, the top right the enhancement of the footprint by the long-range collisions. The bottom left picture demonstrates that an ideal wire reduces the footprint to a size equal to or even smaller than that for head-on collisions only. The compensation still works even with a significant static strength error, as illustrated in the last picture.

Diffusion rates are calculated by launching groups of 100 particles at identical start amplitudes in the horizontal and vertical plane, but with random initial betatron phase. The spread in linear action values is averaged over 1000 consecutive turns to reduce fluctuations due to regular

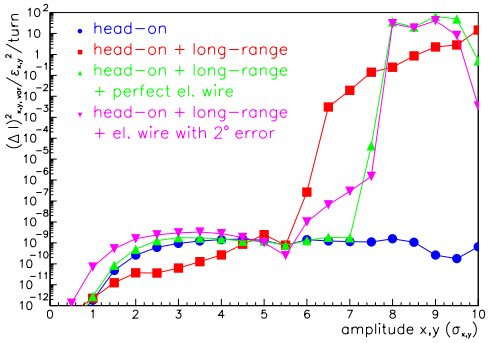

Figure 2: The diffusion per turn as a function of the start amplitude. Different cases are compared.

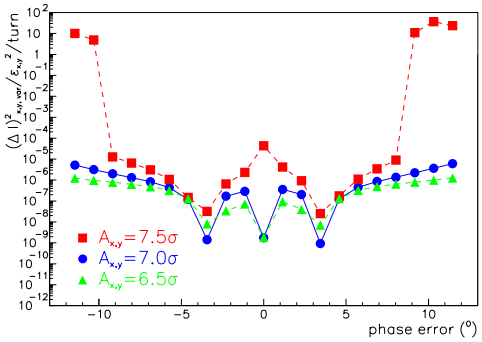

Figure 3: Variation of diffusion rate with symmetric betatron phase error at various amplitudes. The phase errors for the wires on either side and for the two planes are all assumed to be equal.

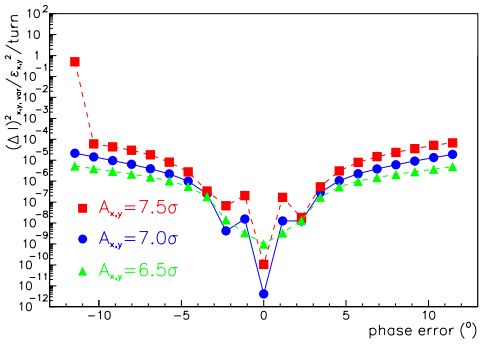

Figure 4: Variation of diffusion rate with betatron phase error at various amplitudes, if there is a compensating wire only on one side of each IP.

phase deformations, and to more clearly pronounce chaotic behavior. The mean increase per turn in the action variance measures the strength of the diffusion.

Figure 2 shows the simulated diffusion rates as a function of start amplitude. The vertical axis is on a logarithmic scale. It represents the increase in the action variance per turn, in units of the rms design emittance. Any value larger than 10^{-8} could indicate a significant diffusion over 10^8 turns. It is most noteworthy, that at an amplitude of about 6σ the diffusion rate increases by 7–9 orders of magnitude, if long-range collisions are present (the red curve, squares). The strong diffusion is absent when only head-on collisions are accounted for (the blue curve, circles). This is consistent with the results of Ref. [2]. When the electric compensating wire is added (green curve, upright triangles), the amplitude of the steep increase moves outwards by 1.5–2σ, to about 7.5–8σ. This remarkable improvement confirms the efficiency of the wire. Even with an imperfect wire (2° phase error - the pink curve, inverse triangles), the diffusion rates in the intermediate amplitude range 6–8σ is still several orders of magnitude lower than without the wire. Note that a 2σ improvement of the dynamic aperture, in both planes, might greatly improve the operating margin of the LHC.

That the wire compensation fails for amplitudes larger than 8σ is understandable. At amplitudes above 8σ the particles start passing through the core of the opposing beam, where the beam force strongly deviates from the $1/r$ force of the wire.

Figure 3 shows a more systematic study of the effect of a phase error. The same phase error with respect to the head-on collision point was assumed for the wires on either side of the IP and in both planes. Results are compared for three different amplitudes. Since, for phase errors of about $\pm 10°$, the diffusion rate at 7.5σ increases to the uncompensated level, we may consider this value as the phase tolerance. In practice, the phase errors are confined to less than $2 \pm 1°$ [4], *i.e.*, phase errors due to optical imperfections will have a negligible effect on the beam-beam compensation.

Alternatively, we consider the case that there is only one wire per IP and study the sensitivity to betatron phase errors in this configuration. The results are shown in Fig. 4. They are similar to, or even lower than, those in Fig. 3, despite of the reduced symmetry. Since it is not possible to choose a location with a phase error less than $1°$ also here we take $\pm 10°$ as the tolerance. The differences in the diffusion rates for one and two wires depend on the working point.

If the wire current is not perfect, the compensation degrades. This is studied in Fig. 5 (again for two wires per IP), depicting diffusion rates at 6.5, 7 and 7.5 σ as a function of the wire strength error in percent. Especially at the largest amplitude, the dependence is rather erratic, presumably indicating the existence of resonance islands. Static strength errors in the range between 0 and -10% appear acceptable.

The effect of a random change in the wire strength from turn to turn is illustrated in Figs. 6 and 7. The strength of

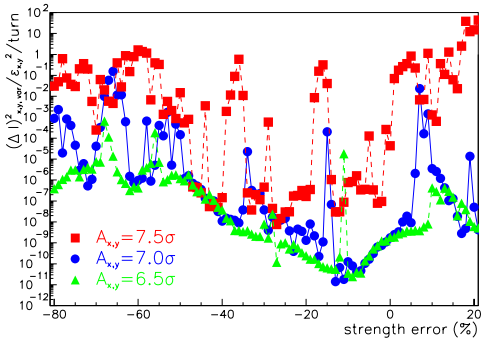

Figure 5: Variation of diffusion rate with static wire strength error (in units of percent) at various amplitudes.

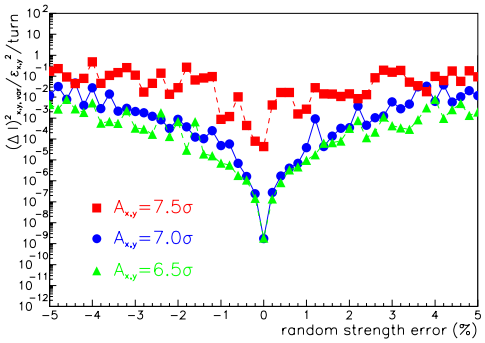

Figure 6: Variation of diffusion rate with peak value of turn-to-turn random wire strength error at various amplitudes. The dipolar deflection by the wire is subtracted including its fluctuation.

.

each wire is assumed to fluctuate from turn to turn. Plotted along the horizontal axis is the normalized peak value $\Delta I_w/I_w$ of the random fluctuation in wire current. The latter is uniformly distributed between $-\Delta I_w$ and ΔI_w. Then the diffusion rates should be symmetric around zero, and deviations from the mirror symmetry reflect the uncertainty of the simulation result, due to the choice of random seed.

In the simulation of Fig. 6, we have assumed that the fluctuation in wire strength does not give rise to dipolar deflections. This means, that in Eq. (6) all three terms containing the factor $\theta_{c,w}$ were varied simultaneously. For the corresponding results in Fig. 7, only the average dipole deflection, *i.e.*, not including the fluctuating part, was subtracted from the wire force. In this case, the beam experiences random dipole kicks in addition to fluctuating focusing forces, and higher order terms. Since no fast orbit feedback is foreseen for the LHC at top energy the second simulation is more realistic. The difference in the computed diffusion rates is small, however, which suggests that the random quadrupolar excitation is more harmful than the dipolar one. Both figures indicate that the tolerance on the turn-to-turn stability of the wire is less than 0.1%.

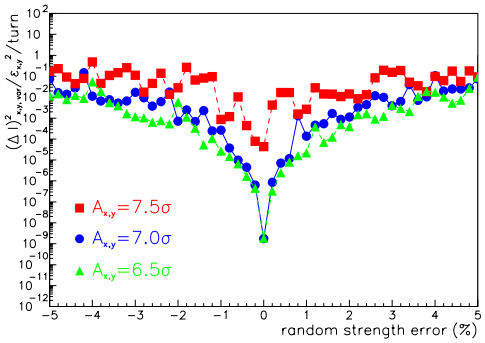

Figure 7: Variation of diffusion rate with random wire strength error at various amplitudes. The average dipole deflection is subtracted.

.

Finally, Fig. 8 shows simulated diffusion rates as a function of an error in the transverse distance between beam and wire. We observe that errors in the wire position towards larger amplitudes are preferred, presumably because the $1/r$ field increases strongly in the vicinity of the thin wire. Note that the sharp increase in the diffusion rates for smaller distances is consistent with the steep rise at an amplitude of 7.5σ, in Fig. 2, and that the preservation of a low diffusion rate for distances 10–20% larger than nominal is compatible with the dependence on the static strength error in Fig. 5. We deduce from Fig. 8 that the tolerable range of distances extends approximately between 0 and 20% of the optimum distance.

In LHC operation, the relative distance of beam and wire can be determined with sufficient precision by detecting the effect of the wire current on the closed orbit.

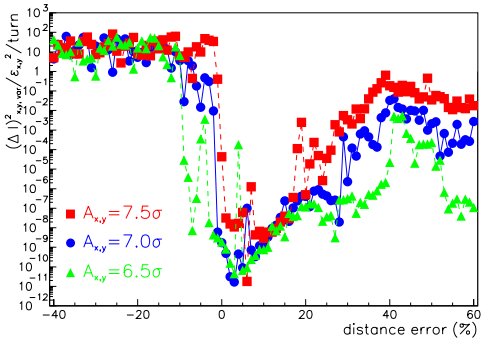

Figure 8: Variation of diffusion rate with wire position error at various amplitudes. Zero on the horizontal axis refers to a beam-wire distance of $(\theta_c/\theta^*_{x,y})\sigma \approx 9.5\sigma$.

4 CONCLUSIONS

Weak-strong simulation studies show that at amplitudes between 6 and 8σ the wire compensation reduces the diffusion rate by many orders of magnitude. The tolerance to betatron phase errors is about 10°. The tolerable range of static strength errors extends between 0 and -10%. Transverse distance errors between 0 and 20% are acceptable. The most critical tolerance appears to be that to turn-to-turn fluctuation of the wire strength. Here a stability better than 0.1% must be achieved.

5 ACKNOWLEDGEMENTS

I thank O. Brüning, W. Herr, J-P. Koutchouk and F. Ruggiero for suggesting this study, support, helpful discussions, and a careful reading of the manuscript.

6 REFERENCES

[1] T. Sen, et al., "Effect of the Beam-Beam Interactions on the Dynamic Aperture and Amplitude Growth in the LHC," CERN-SL-99-039 AP (1999).

[2] Y. Papaphilippou and F. Zimmermann, "Weak-Strong Beam-Beam Simulations for the LHC," Proc. of the Workshop on Beam-Beam Effects in Large Hadron Colliders — LHC99, Geneva, April 12-17, CERN-SL-99-039 AP (1999) (J. Poole and F. Zimmermann eds.); published in Physical Review Special Topics – Accelerators and Beams 2, 104001 (1999).

[3] H. Grote, et al., "LHC Dynamic Aperture at Collision," LHC Project Note 197 (1999).

[4] J.-P. Koutchouk, "Principle of a Correction of the Long-Range Beam-Beam Effect in the LHC using Electromagnetic Lenses," LHC Project Note 223 (2000).

[5] J.-P. Koutchouk, "Correction of the Long-Range Beam-Beam Effect in LHC using Electro-Magnetic Lenses," presented at IEEE PAC 2001 Chicago (2001).

[6] J.-P. Koutchouk, these proceedings.

[7] W. Herr, "Effects of PACMAND Bunches in the LHC," CERN-LHC-Project-Report-39 (1996).

[8] J. Irwin, "Diffusive Losses from SSC Particle Bunches due to Long Range Beam-Beam Interactions," SSC-233 (1989).

Beam Sizes in Collision and Flip-Flop States at KEKB

F. Zimmermann, CERN, Geneva, Switzerland

Abstract

Evaluating a simplified linear model of the beam-beam interaction, self-consistent horizontal beta functions, emittances and beam sizes are computed for the two unequal colliding beams in KEKB. For head-on collisions only one equilibrium solution exists at the nominal tunes. However, if for off-center collisions the quadrupolar component of the beam-beam force becomes defocusing, we obtain two solutions, one of which describes a flip-flop state with increased size of the positron beam. This result may explain observations of sudden luminosity drops.

1 INTRODUCTION

During KEKB operation drops in the luminosity are observed, which are associated with step changes in the horizontal and/or vertical beam sizes at the interaction point (IP) [1]. Often the LER horizontal beam size increases. Changes in the beam size appear to be correlated with small orbit variations. In particular, a hysteresis is observed when the beam-beam separation at the collision point is varied. In this report, we study a simple linear model of the self-consistent horizontal optics and emittances for the two unequal colliding beams, evaluate their dependence on the betatron tune and the beam-beam tune shift, and demonstrate the existence of flip-flop solutions for off-center collisions.

2 SELF-CONSISTENT OPTICS AND BEAM SIZES

In collision, the beam emittance and beta functions are changed by the focusing force of the opposing beam. Neglecting the change in the other beam (weak-strong approximation), the horizontal dynamic beta function, $\beta_{x,1(2)}$, at the collision point is usually obtained as [2]

$$b_{x,1(2)} \equiv \frac{\beta_{x0,1(2)}}{\beta_{x,1(2)}} = \frac{\sin 2\pi(Q_{1(2)} + \Delta Q_{1(2)})}{\sin 2\pi Q_{1(2)}} \quad (1)$$

where

$$Q_{1(2)} + \Delta Q_{1(2)} = \frac{1}{2\pi} \arccos\left(\cos 2\pi Q_{1(2)} - 2\pi\xi_{0,1(2)} \sin 2\pi Q_{1(2)}\right) \quad (2)$$

and $Q_{1(2)}$ denotes the unperturbed horizontal betatron tune of beam 1 (or beam 2). The subindices 1 and 2 refer to the electron (HER) and positron beam (LER), respectively; the subindex '0' signifies the values of beta function and emittance without the focusing effect of the opposing beam.

Table 1: Parameters relevant to the flip-flop analysis.

variable	HER	LER
hor. beam-beam tune shift ξ_x	0.049	0.055
vert. beam-beam tune shift ξ_y	0.025	0.037
hor. tune	44.520	45.505
vert. tune	41.587	43.575
hor. beta function β_{x0}	63 cm	59 cm
vert. beta function β_{y0}	0.7 cm	0.7 cm
vert. beam-beam tune shift ξ_y	0.025	0.037
single-bunch current	0.48 mA	0.63 mA

The parameter $\xi_{0,1(2)}$ is the horizontal beam-beam tune shift, calculated from the unperturbed beta functions and emittances,

$$\xi_{0,1(2)} \equiv \frac{N_{2(1)} r_0}{2\pi\gamma\epsilon_{x0,2(1)}} \frac{\beta_{x0,1(2)}}{\beta_{x0,2(1)}}, \quad (3)$$

where r_0 denotes the classical electron radius. For the parameter values of KEKB, summarized in Table 1, the (inverse) normalized dynamic beta functions evaluate to $b_{x,1} = 2.40$ and $b_{x,2} = 4.78$.

Since the actual beam-beam tune shift, $\xi_{1,2}$, depends on the dynamic beta function, Eq. (1) does not describe a self-consistent solution of the problem. Neither can it account for flip-flop phenomena or for the simultaneous existence of more than one equilibrium state. The flip-flop effect with linearized beam-beam force for round beams was recently analyzed by A. Otboyev and E. Perevedentsev [3], who computed self-consistent beta functions and equilibrium emittances. We here follow and extend their formalism, and then apply it to the KEKB case of flat beams with unequal parameters. For simplicity, we limit the discussion to the horizontal plane, in which flip-flop effects are frequently observed.

The basic equations governing the evolution of the beta functions are [3]

$$b_1^2 = 1 + 2c_1 x_1 \frac{b_2}{e_2} - x_1^2 \frac{b_2^2}{e_2^2} \quad (4)$$

$$b_2^2 = 1 + 2c_2 x_2 \frac{b_1}{e_1} - x_2^2 \frac{b_1^2}{e_1^2} \quad (5)$$

were $c_{1(2)} \equiv \cot(2\pi Q_{1(2)})$, $b_{1(2)} \equiv \beta_{x0,1(2)}/\beta_{x,1(2)}$, $x_{1(2)} \equiv 2\pi\xi_{0,1(2)}$, and $e_{1(2)} \equiv \epsilon_{x,1(2)}/\epsilon_{x0,1(2)}$.

Figure 1 displays the graphical method [4] of solving Eqs. (4) and (5). Plotting the two curves $b_1(b_2)$ and $b_2(b_1)$,

solutions to (4) and (5) are given by their intersections. As can be seen, for the parameters considered and for constant emittances, $e_1 = e_2 = 1$, there is only one intersection and, hence, no flip flop is expected. Figure 2 shows an equivalent picture obtained by neglecting the quadratic terms in (4) and (5). The difference to Fig. 1 is insignificant.

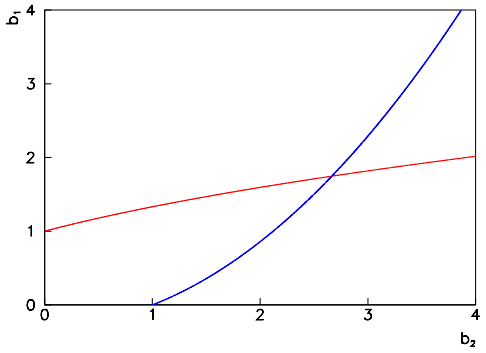

Figure 1: Graphical solution of the complete Eqs. (4)–(5) for constant emittances, $e_{1(2)} \equiv \epsilon_{x,1(2)}/\epsilon_{x0,1(2)} = 1$. Plotted is the variation of the inverse electron beta function, $b_1 = \beta_{x0,1}/\beta_{x,1}$, as a function of the inverse positron beta function, $b_2 = \beta_{x0,2}/\beta_{x,2}$, for the parameters of Table 1.

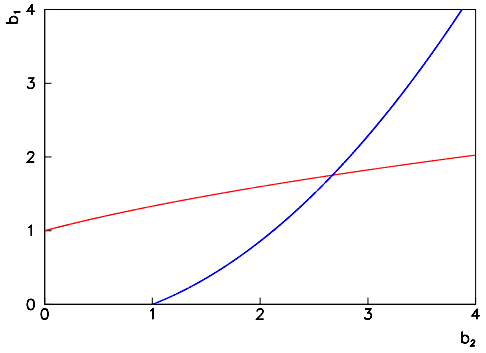

Figure 2: Graphical solution of Eqs. (4)–(5), considering only the terms proportional to $c_{1(2)}x_{1(2)}$, for constant emittances, $e_{1,2} \equiv \epsilon_{x,1(2)}/\epsilon_{x0,1(2)} = 1$. Plotted is the variation of the inverse electron beta function, $b_1 = \beta_{x0,1}/\beta_{x,1}$, as a function of the inverse positron beta function, $b_2 = \beta_{x0,2}/\beta_{x,2}$, for the parameters of Table 1.

If the beams collide with a horizontal offset, the quadrupolar component of the beam-beam force may change sign. Figure 3 shows the graphical solution for an unperturbed beam-beam tune shift parameter ξ_0 equal to $-1/4$ times the nominal value. Still there is only one intersection.

Next we include the variation in emittance. Following Ref. [5], or ignoring the oscillatory term in the solution

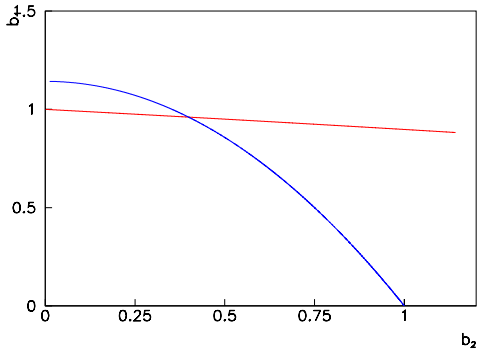

Figure 3: Graphical solution of Eqs. (4)–(5) for constant emittances, $e_{1,2} \equiv \epsilon_{x,1(2)}/\epsilon_{x0,1(2)} = 1$, assuming a negative beam-beam tune shift $\xi_{0,1(2)} = -0.25\xi^{\rm nom}_{0,1(2)}$, where $\xi^{\rm nom}_{0,1(2)}$ represents the nominal value listed in Table 1. Plotted is the variation of the inverse electron beta function, $b_1 = \beta_{x0,1}/\beta_{x,1}$, as a function of the inverse positron beta function, $b_2 = \beta_{x0,2}/\beta_{x,2}$.

of Ref. [3], the emittance changes with the strength of the beam-beam focusing according to

$$e_{1(2)} = \frac{1 + p_{1(2)} \cot 2\pi Q_{x,1(2)}}{\sqrt{1 + 2p_{1(2)} \cot 2\pi Q_{x,1(2)} - p^2_{1(2)}}}, \qquad (6)$$

where $e_{1(2)} \equiv \epsilon_x, 1(2)/\epsilon_{x0,1(2)}$ and $p_{1,2} \equiv x_{1,2}b_{2,1}/e_{2,1}/b_{1,2}$. This equation is illustrated in Fig. 4.

Figures 5 and 6 shows a more precise SAD computation of the dynamic emittances and beta functions as a function of the beam-beam tune shift, provided by H. Koiso, which accounts for the exact ring optics. The emittance variation in Fig. 5 agrees within 10% with the simplified estimate of Eq. (6) and Fig. 4.

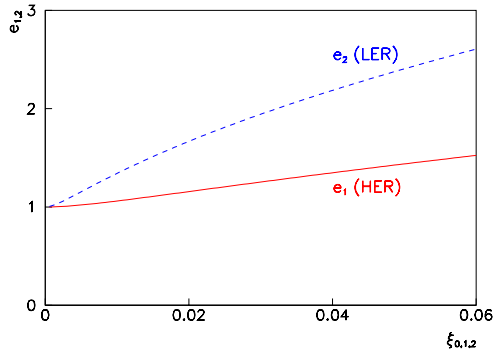

Figure 4: Horizontal emittance $e_{1,2}$ in the high energy and low energy ring as a function of beam-beam parameter $\xi_{1,2}$, for constant values of $b_{2,1} = e_{2,1} = 1$, according to Eq. (6).

From Figs. 4 and 5, we approximate the dependence of the horizontal emittances on the beam-beam lens by the

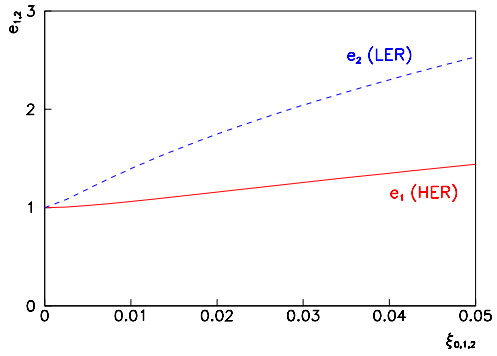

Figure 5: Dynamic emittance in units of the unperturbed emittance, $e_{1,2}$, as a function of beam-beam tune shift for the low and high-energy rings of KEKB, computed by SAD. (Courtesy H. Koiso)

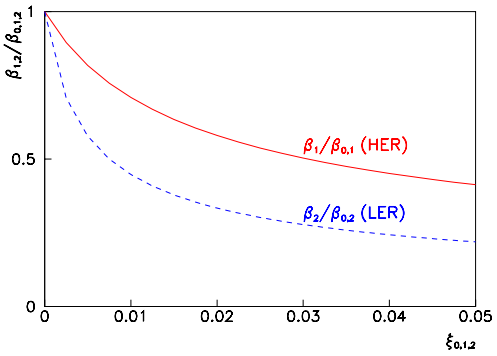

Figure 6: Horizontal beta functions $\beta_{1,2}/\beta_{0,1,2} \equiv 1/b_{1,2}$ as a function of beam-beam tune shift for the low and high-energy rings of KEKB, computed by SAD. (Courtesy H. Koiso)

linear relations

$$e_1 \approx 1 + k_1 x_1 \frac{b_2}{b_1 e_2}, \quad (7)$$

$$e_2 \approx 1 + k_2 x_2 \frac{b_1}{b_2 e_1}, \quad (8)$$

where, for the nominal tunes (subindex 0), $k_1 = k_{0,1} \approx 1.3$, and $k_2 = k_{0,2} \approx 4.6$. The reason why the values of $k_{0,1}$ and $k_{0,2}$ are so different is that in the LER the horizontal tune is much closer to the half integer resonance (see Eq. (6) and Table 1). Note that the equation for $e_{1(2)}$ also contains the beta function $b_{1(2)}$, which is an extension of the formulae in Ref. [3] that naturally follows from Eq. (6) inserting the definitions of $p_{1,2}$ and $x_{1,2}$. Equations (7) and (8) are approximations, which could be refined in future studies.

We can solve the two equations (7) and (8) for $e_{1,2}$:

$$e_1 = \frac{1}{2}\left(1 + k_1 x_1 \frac{b_2}{b_1} - k_2 x_2 \frac{b_1}{b_2}\right) + \sqrt{\frac{1}{4}\left(1 + k_1 x_1 \frac{b_2}{b_1} - k_2 x_2 \frac{b_1}{b_2}\right)^2 + k_2 x_2 \frac{b_1}{b_2}},$$

$$e_2 = \frac{1}{2}\left(1 + k_2 x_2 \frac{b_1}{b_2} - k_1 x_1 \frac{b_2}{b_1}\right) + \sqrt{\frac{1}{4}\left(1 + k_2 x_2 \frac{b_1}{b_2} - k_1 x_1 \frac{b_2}{b_1}\right)^2 + k_1 x_1 \frac{b_2}{b_1}}.$$

Inserting these expressions into Eqs. (4) and (5), we may once again use the graphical method to determine the remaining two unknowns b_1 and b_2.

Figure 7 shows the solution for the nominal parameters of Table 1. There is only one intersection, which indicates a unique equilibrium. The curves look similar to those in Fig. 1, which were computed for constant emittances.

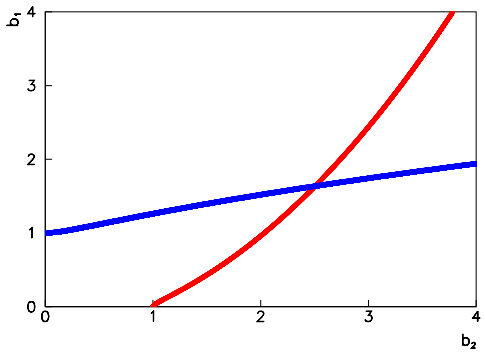

Figure 7: Graphical solution of Eqs. (4)–(5) for emittances that vary linearly with the strength of the beam-beam force as in Eqs. (7) and (8). Plotted is the electron beta function, $b_1 = \beta_{x0,e}/\beta_{x,e}$, as a function of the positron beta function, $b_2 = \beta_{x0,p}/\beta_{x,p}$, for the nominal parameters of Table 1.

The situation changes dramatically, if we invert the sign of the beam-beam tune shift, in order to model a situation with off-center collisions. Figure 8 illustrates a typical example, where we consider an unperturbed tune shift equal to $-0.25\ \xi^{\rm nom}_{0,1(2)}$. In this case there are two intersections, *i.e.*, two solutions. This is quite different from the result for constant emittances in Fig. 3. One of the two solutions represents a large increase of the positron beta function (small value of b_2), possibly consistent with the observed flip-flop state.

The self-consistent beta functions and emittances depend on the tunes of both beams. Figures 9 and 10 illustrate the dependence of the normalized beam sizes $\sigma_{x,1(2)}/\sigma_{x0,1(2)} = \sqrt{e_{1(2)}/b_{1(2)}}$ on the tunes in either ring, respectively, for the nominal beam-beam tune shift. In this calculation, we have approximated the variation of the coefficients k_1 and k_2 in Eqs. (7) and (8) with the tunes $Q_{1,2}$

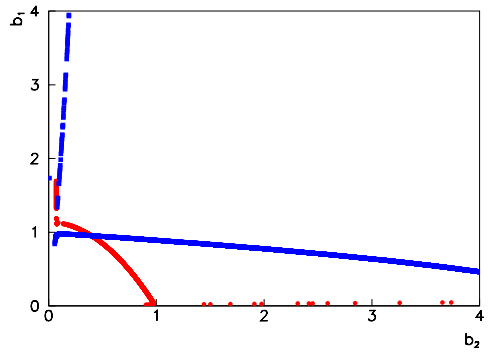

Figure 8: Graphical solution of Eqs. (4)–(5) assuming a negative beam-beam tune shift $\xi_{0,1(2)} = -0.25\xi^{\rm nom}_{0,1(2)}$, for emittances that vary linearly with the strength of the beam-beam force as in Eqs. (7) and (8). Plotted is the electron beta function, $b_1 = \beta_{x0,e}/\beta_{x,e}$, as a function of the positron beta function, $b_2 = \beta_{x0,p}/\beta_{x,p}$.

as

$$k_{1(2)} \approx k_{0,1(2)}\cot(2\pi Q_{1(2)})/\cot(2\pi Q_{0,1(2)}). \quad (9)$$

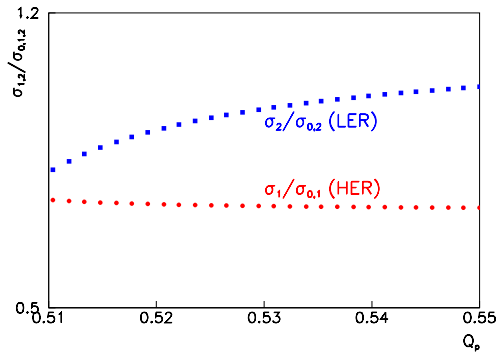

Figure 9: Self-consistent horizontal beam sizes σ_x/σ_{x0} as a function of the positron tune (right). The positron tune is set to 0.505.

An offset between the two beams at the collision point distorts the closed orbit, introduces a change in the linear focusing, and excites additional higher-order resonances. As indicated earlier in this paper, we only consider the variation in the quadrupolar focusing force, and approximate the change in the focusing due to a varying beam-beam separation by a common multiplication factor M_ξ for the two beam-beam tune shift parameters. This is based on the assumption that a small beam-beam offset reduces the strength of linear focusing experienced at the collision point by a similar factor for either beam, provided the sizes of the two beams are equal (note that they will not remain equal once a flip-flop state is established). For larger offsets, the beam-beam focusing force changes sign, which we model by a negative value for M_ξ.

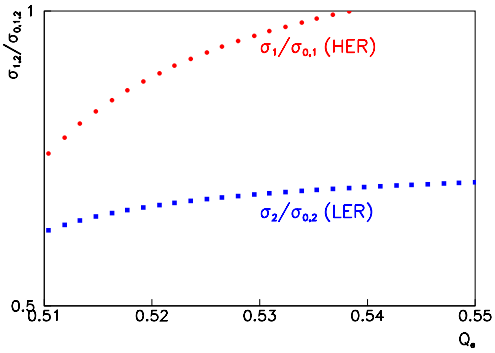

Figure 10: Self-consistent horizontal beam sizes σ_x/σ_{x0} as a function of the positron tune. The electron tune is set to 0.520.

Figures 11–13 illustrate the dynamic variation of beta function, emittances and beam sizes as a function of a positive multiplication factor M_ξ. The beta functions decrease more strongly than the emittances increase as a function of the beam-beam tune shift, such that the IP beam sizes shrink for higher current. Equivalent results for a negative multiplication factor M_ξ are shown in Figs. 14–16. Consistent with Fig. 3, in the latter case two solutions coexist. The additional solution appears to be of the flip-flop type. It is characterized by a large increase in the LER IP beta function (Fig. 14), a decrease in the emittance (Fig. 15) and a resulting net growth of the IP beam size (Fig. 16).

A tentative explanation of the observed hysteresis may then be the following. For a sufficiently large beam-beam offset of about $2\sigma_x$, the 'quadrupolar' component of the horizontal beam-beam force changes sign, *i.e.*, the force becomes defocusing instead of focusing, and there emerges a new equilibrium, which represents a flip-flop state. Therefore, repeated changes in the sign of ξ — due to varying beam-beam separation —, might induce transitions between the different solutions that exist for $\xi < 0$.

3 CONCLUSIONS

Calculations of horizontal equilibrium sizes for head-on colliding beams at KEKB suggest the existence of a unique equilibrium solution. If the beams are horizontally separated sufficiently far that the 'quadrupolar' component of the beam-beam force is defocusing, two self-consistent solutions coexist, one of which describes a flip-flop state, in which the positron beam is blown up. This appears consistent with some of the observations.

Our analysis was based on a simplified model, which considers only the horizontal plane, a linearized beam-beam force, a linear dependence of the emittance on the beam-beam tune shift, and a common scale factor for both beam-beam parameters representing the effect of a trans-

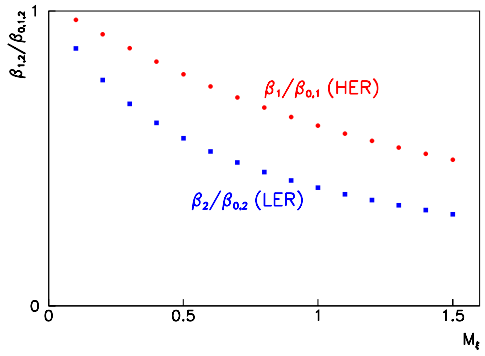

Figure 11: Self-consistent dynamic beta functions $\beta_{1,2}/\beta_{0,1,2} \equiv 1/b_{1,2}$, as a function of a common positive multiplication factor M_ξ for both tune shift parameters. This multiplication factor is intended to model a change in linear focusing arising from a beam-beam offset. The tunes are set to 0.520 (HER, e^-) and 0.505 (LER, e^+), respectively.

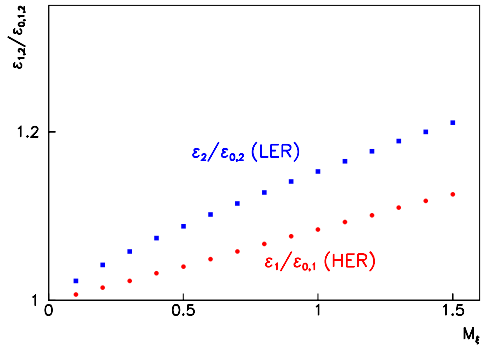

Figure 12: Self-consistent dynamic emittances $e_{1,2} \equiv \epsilon_{1,2}/\epsilon_{0,1,2}$, as a function of a common positive multiplication factor M_ξ for both tune shift parameters. This multiplication factor is intended to model a change in linear focusing arising from a beam-beam offset. The tunes are set to 0.520 (HER, e^-) and 0.505 (LER, e^+), respectively.

verse offset. All of these approximations could be improved. Future extensions might also include the vertical plane, bunch length and crossing angle, as well as the nonlinear components of the force including an arbitrary beam-beam separation.

4 ACKNOWLEDGEMENTS

I thank K. Oide for suggesting this study, H. Fukuma, Y. Funakoshi, H. Koiso, K. Ohmi, K. Oide, and J. Urakawa for the hospitality at KEK and for helpful discussions, W. Herr and F. Ruggiero for their support, and the organizers and participants of the FNAL 2001 beam-beam workshop, especially T. Sen and M. Xiao, for their interest in this work.

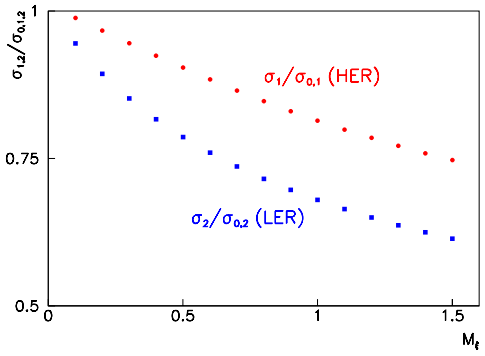

Figure 13: Self-consistent dynamic beam sizes $\sigma_{1,2}/\sigma_{0,1,2} \equiv \sqrt{e_{1,2}/b_{1,2}}$, as a function of a common positive multiplication factor M_ξ for both tune shift parameters. This multiplication factor is intended to model a change in linear focusing arising from a beam-beam offset. The tunes are set to 0.520 (HER, e^-) and 0.505 (LER, e^+), respectively.

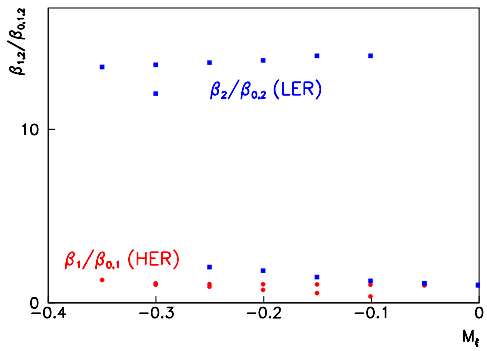

Figure 14: Self-consistent dynamic beta functions $\beta_{1,2}/\beta_{0,1,2} \equiv 1/b_{1,2}$, as a function of a common negative multiplication factor M_ξ for both tune shift parameters. This multiplication factor is intended to model a change in linear focusing arising from a beam-beam offset. The tunes are set to 0.520 (HER, e^-) and 0.505 (LER, e^+), respectively.

5 REFERENCES

[1] K. Oide, private communication; and M. Tawada, this workshop (2001).

[2] M. A. Furman, "Beam-beam tune shift and dynamical beta function in PEP-II," LBL-34957, EPAC 94, London (1994).

[3] A.V. Otboyev and E.A. Perevedentsev, "Self-Consistent Beta Functions and Emittances of Round Colliding Beams," PRST-AB 2, 104401 (1999).

[4] A.B. Temnykh, INP Report No. INP 82-148 (1982).

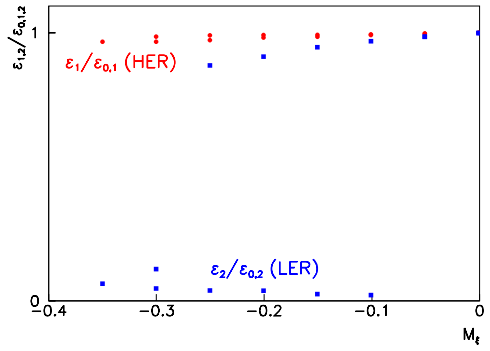

Figure 15: Self-consistent dynamic emittances $e_{1,2} \equiv \epsilon_{1,2}/\epsilon_{0,1,2}$, as a function of a common negative multiplication factor M_ξ for both tune shift parameters. This multiplication factor is intended to model a change in linear focusing arising from a beam-beam offset. The tunes are set to 0.520 (HER, e^-) and 0.505 (LER, e^+), respectively.

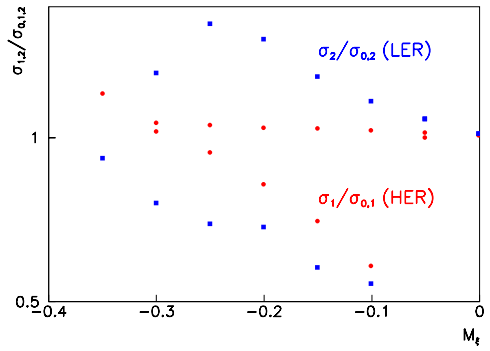

Figure 16: Self-consistent dynamic beam sizes $\sigma_{1,2}/\sigma_{0,1,2} \equiv \sqrt{e_{1,2}/b_{1,2}}$, as a function of a common negative multiplication factor M_ξ for both tune shift parameters. This multiplication factor is intended to model a change in linear focusing arising from a beam-beam offset. The tunes are set to 0.520 (HER, e^-) and 0.505 (LER, e^+), respectively.

[5] K. Hirata and F. Ruggiero, LEP Note 611 (1988).

[6] K. Yokoya, Y. Funakoshi, E. Kikutani, H. Koiso, and J. Urakawa, KEK Preprint 89-14 (1989).

[7] Y. Alexahin, "A Study of the Coherent Beam-Beam Effect in the Framework of the Vlasov Perturbation Theory," CERN-LHC-Project-Report-461, submitted to NIM A (2001).

Summary of session on beam-beam compensation schemes

W. Herr CERN, SL Division

Abstract

This paper summarizes the presentations and discussions in the session on beam-beam compensation held during the workshop on beam-beam effects at Fermilab on 25 to 27 June 2001. The presentations and discussion were focused on two main topics: linear and non-linear compensation with electron lenses in the Tevatron and a compensation scheme for long-range effects in the LHC using a pulsed wire.

1 INTRODUCTION

In high luminosity hadron colliders the beam-beam effect eventually limits the bunch intensities. Recently schemes have been proposed to compensate part of the detrimental effects. During this session three presentation were made:

- Correction of the long-range beam-beam effect in LHC using electromagnetic lenses; by J.P. Koutchouk, CERN
- Simulation of the LHC long-range compensation; by F. Zimmermann, CERN
- Study of the Tevatron compensation; by D. Shatilov, BINP

The presentations were discussed and some issues of general interest for beam-beam compensation that were raised during this session are presented here.

2 COMPENSATION OF LONG-RANGE EFFECTS

Recently the long-range beam-beam effects have been more and more recognized as important factors for the stability of the beams in lepton and hadron colliders. Both, active or passive compensation of at least part of these effects may be essential for machines with many bunches.

2.1 Pulsed wire for compensation of long range effects

The proposal to compensate the long-range beam-beam effects (LRE) was made after initial tracking studies have shown the importance of long-range effects on the dynamic aperture. It was realized that for large enough beam separation the long range forces decrease with $\frac{1}{r}$, where r is the distance between the beams. Such a field can also be produced by a thin wire. For the bulk of the long-range encounters this assumption is valid and the separation is typically between 7 and 10 σ. Furthermore, most of these encounters happen where the beams are still approximately round and at a phase advance of $\frac{\pi}{2}$ from the collision point. It can therefore be justified to lump all interactions into a single one. The linear part of the long range forces is largely compensated by the alternating crossings in the LHC interaction points. The size of the beam-beam tune-spread (footprint) can be strongly decreased [1] by a wire running along the beam. The current times length of such a wire requires approximately 80A $\cdot$ 1m. The size of the footprint can be decreased by a factor 10. Effects on the closed orbit are corrected simultaneously.

The bunch filling scheme of the LHC causes a difficulty, producing so-called PACMAN bunches which experience only part of the beam-beam effect and therefore need only part of the correction. To account for this it is proposed to pulse the current in the wire at the beginning and end of a batch, i.e. produce smaller compensating fields for the PACMAN bunches.

Preliminary considerations have shown that such a scheme is technically possible, using commercially available equipment.

The wire is operated in the vacuum of the machine and therefore needs a cooling system. Such a cooling is technically difficult for a wire of 1 mm diameter and alternatives have been proposed where a much thicker wire with cooling inside is used and the surface of the wire is shaped to obtain the correct $\frac{1}{r}$ dependence.

2.2 Simulation of long range compensation with pulsed wire

To evaluate the above compensation scheme, a study was launched to simulate the effect on the beam. A second aim was to work out the tolerances and the sensitivity of the proposed setup to imperfections. For that purpose a weak-strong simulation was developed, assuming a linear transport in the arcs and at the interaction point a head-on collision and on both sides long-range collisions together with a wire. The wire was assumed at a distance of 9.5 σ and producing a $\frac{1}{r}$ force. The tests were made on possible betatron phase errors, as well as on wire positioning and strength errors. For the evaluation the footprints and the diffusion rate was used. Without errors the footprints were reduced almost to the size of the head-on footprints alone since the compensation in the program is almost perfect. Already in earlier studies it was shown that the dif-

fusion rate increases steeply for particle amplitudes above 6σ (witout wire). With a wire the increase of the diffusion sets in about 1.5 to 2 σ later, i.e. a significant increase of the available stable region. With phase errors of 2^o to the wire, the improvement is still 1 to 1.5 σ. Only for errors larger that 10^o the original steep increased is observed again. However such phase errors are not expected for a reasonably well behaved insertion optics. Studying the effect of static wire strength errors it was found that errors in the range [-40%, +20%] still give a good correction.

The positioning of the wire with respect to the beam is an important issue that may need some further thoughts, a consensus reached during the discussion. The simulation of positioning errors in the range [-40%, +60%] showed a dependence with acceptable compensation in the interval [-5%, +40%]. I.e. in case of positioning errors, an error away from the beam is preferable. While studying a scheme with a single wire compensating the long-range effects from both sides of the interaction point, it was shown that a scheme with two separate wires has advantages.

During the discussion it was agreed that no obstacle was identified up to now and the participants of the workshop strongly recommend to continue with this scheme.

3 STUDY OF TEVATRON COMPENSATION

Another simulation study aimed to evaluate the linear and non-linear compensation with electron lenses in the Tevatron, and possibly to define some strategies for the operation. For that purpose a weak-strong beam-beam code was developed (LIFETRAC) for the Tevatron that is fully symplectic in 6D and can use various noise sources, such as tune modulation or beam separation at the collision point.

The main purpose of the linear beam-beam compensation is to suppress the bunch-to-bunch tune spread in the Tevatron. In a first step, good and bad working points are determined with the program. In the second step all bunches at bad working points are moved to the good working points with linear electron lenses. varying the parameters of the lenses and including perturbations this strategy can be tested. After the application of the linear lenses, the distributions of antiprotons at originally bad working points are practically the same as on good working points. Different electron lens profiles were investigated, studying the antiproton tune-shift and the luminosity. The difference was found to be rather small. Injecting noise on the electron beam led to exponential emittance growth.

The purpose of the non-linear compensation is to reduce the intrabunch tune spread, i.e. the tune footprint. The footprint of long range beam-beam interactions show a characteristic 'folding' for particles at amplitudes close to the beam separation. If this appears close to low order resonances it is considered dangerous since there we have $\frac{dQ}{dA} \approx 0$. Bad lifetime of tails must be expected. The effect of the non-linear lens is to scale down the footprint, thus moving the folding over area to smaller particle amplitudes. This may now lead to a blowing up of the core of the bunches that must be avoided. The recommended procedure now used in the simulation is to reduce the footprint moderately, i.e. by a factor of two in the first step. A linear lens should then be used to shift the bunch to a better working point where the reduced footprint is in an area free of dangerous resonances. Therefore the non-linear and linear compensation must be applied simultaneously.

In the discussion it was achnowledged that the study helped to understand better the requirements and to define the parameters for the compensation. However more experimental data is desirable. While the linear compensation looks very promising, it is recommended to further study the non-linear compensation. A consensus was reached that a small tune footprint (i.e. tune spread) alone does not guarantee a safe running. It must be considered a necessity but it is not sufficient.

4 CONCLUSIONS

Compensation schemes for head-on as well as for long range beam-beam effects have been discussed. Both approaches were found promising and well under way and the workshop strongly recommends to continue.

5 REFERENCES

[1] J.P. Koutchouk; *Correction of the Long-Range Beam-Beam Effect in LHC using Electromagnetic Lenses* ; Proc. Particle Accelerator Conference 2001, (Chicago, 2001).

[2] F. Zimmermann; *Simulation of the LHC Long-Range Compensation*; Proc. workshop on beam-beam effects 2001, (FNAL, 2001).

[3] D. Shatilov; *Study of the Tevatron Compensation*; Proc. workshop on beam-beam effects 2001, (FNAL, 2001).

Summary of the Session on Weak-Strong Phenomena

J.P. Koutchouk, CERN, Geneva, Switzerland

Abstract

This session took place June 26th in the afternoon, with the participation of (by memory) Y. Alexahin, M. Boscolo, A. Burov, N. Gelfand, J.P. Koutchouk, F. Schmidt, Y. Shatunov, V. Shiltsev, M. Syphers, T. Sen, M. Xiao, F. Zimmermann. The charge to this session as foreseen by the organizers was

- to review the present understanding of the weak-strong phenomena in general
- and more specifically the performance limitations of the Run II of the Tevatron,
- to review, propose and prioritize experiments crucial to Run II, LHC, CESR and VLHC.

1 INTRODUCTION

This summary is organized as follows:

- The talks given in the session are briefly summarized together with the discussions which arose,
- An attempt is made at comparing the evolution of the understanding and of the outstanding questions over the last few beam-beam workshops,
- A list of proposed actions is submitted.

2 SUMMARY OF THE TALKS AND DISCUSSIONS

2.1 VLHC Proposal, by M. Syphers/FNAL

This proposal is now an official Fermilab document Fermilab TM2149, June 4th 2001 and can be consulted on the Web. The main feature of this proposal is a big tunnel to house initially a 40 TeV machine and later a 200 TeV machine. Two experimental points are foreseen. A selection of parameters relevant to the beam-beam effect is given in Table 1. The beam aspect ratio at the IP's (round or flat) is not yet decided. As commented by the author, the parameters of the beam-beam interactions in the VLHC proposal are comparable to those of Run II and LHC and actually less demanding.

Energy	TeV	40	200
Luminosity		10^{34}	$2\ 10^{34}$
β^*	m	.3	.71
σ_s	m	.03	.08
ξ/IP		$\approx$ .003	.008
# LR interactions	comparable to Run II and LHC		
LR separation	σ	10	
Rad damping	hour	many	1

Table 1: A selection of VLHC Parameters

The recent findings on Run II and LHC show however that a long-range beam-beam separation of 10 σ is insufficient. These machines will have to live with this limitation. It is recommended to increase this separation in a new design. The target value is presently not clear, perhaps as large as 15 σ.

2.2 Tracking for LHC, by F. Schmidt/CERN

The issues in tracking with the beam-beam effect is an accurate model of the physical phenomena and tracking over long times. For LHC, the tracking is carried out in 6D except for the b-b lens which is 4D. The tracking time has been increased from 10^5 to 10^6 turns (89 s in accelerator time). The average beam separation at the LR interaction points is 14 σ at injection and 9.5 σ in collision. The main results are summarized in table 2. The conclusions that can be drawn from this study are:

	Injection	Collision
no beam-beam	$\geq$12	$\geq$12
with beam-beam, 10^5 turns	$\geq$9	$\geq$6
with beam-beam, 10^6 turns	$\geq$7	$\geq$5
onset of chaos	7	4.5

Table 2: Dynamic aperture in LHC in σ

- As already observed in former studies, the long range beam-beam effect is indeed the limiting phenomenon. It is significantly stronger than the machine non-linearities.
- The few places where the beam separation is only 7 σ in collision do play a significant role.
- The phenomenology resembles that of a tune modulation. Particles may be lost after 10^5 turns, i.e. on a long time scale. What happens after 10^6 turns?
- With the nominal machine parameters, the LHC dynamic aperture in presence of the beam-beam interaction might be too small.
- The tune spread at 12 σ at injection due to the LR interactions is only 0.001. It is clearly uncorrelated with the dynamic aperture. The onset of chaos, though not always easy to identify, seems well correlated.

2.3 *Tracking for Run IIa, by M. Xiao/FNAL*

In Run IIa, the numbers of bunches is significantly increased to increase the luminosity while reducing the number of events per collision. Each beam is made of 3 trains of 12 bunches, i.e. 36 bunches instead of 6 in Run I. The tracking scenario includes two head-on collision and 70 long-range interactions. The beam separation is 10 σ except at 4 places where it is only 6 σ.

After discussion it appears that the tracking is 4D only. This is OK for the footprints. For the dynamic aperture however, without the synchrotron modulation, its results should be interpreted as optimistic. Yet, the tracking results show a drastic effect of the long-range interactions:

- The footprint of the PACMAN bunches is shifted by 0.01.
- The LR interactions increase the footprint by 60% (comparable to LHC).
- The dynamic aperture decreases from 12 to 6 σ at 10^6 turns (again comparable to LHC).
- A tune diffusion is noticeable for amplitude from 2 σ onwards.

A crossing angle (4D, with beam slicing) improves the dynamic aperture by 1 to 2 σ, with some reduction of the luminosity.

Altogether, although the physics is not exactly the same (the long-range interactions are spread in betatron phase all around the Tevatron), the LHC and Run IIa tracking results show significant similarities. In both cases, the beam separation of 10 σ appears too small. The footprint criterion which revealed to be the significant non-linear parameter for the head-on collisions does not hold in presence of long-range interactions. The 4D on-momentum tracking does not incorporate dispersion-related phenomena analysed in the next talk.

2.4 *Synchro-betatron Coupling, by Y. Alexahin/FNAL*

This study is analytic and the quantitative results based on perturbation theory. Three families of phenomena are studied:

- The beam-beam *chromaticity*: due to the non-vanishing dispersion at the long-range interaction points, the chromaticity is perturbed by the residual sextupolar field of the exciting beam. The chromaticity spread due to the amplitude spread is as large as 14 units. This seems to be probably just acceptable at the Tevatron.
- Odd-order resonances close to the nominal working point are excited. Calculations show that the 5th order family together with its synchrotron satellites overlap, creating the condition of a diffusion of the particles from the core of the beam.
- A shorter bunch length causes synchrotron satellites of even order resonances (12th order) to be broadened. The resonance lines remain separated with the Cu RF system. The stronger Sc RF system causes the high Qs resonances to overlap.

Yuri advocates to change the nominal working point to .685/.675 to minimize the excitation of the 5th order resonances. The other effects seem rather drastic and likely to limit the performance in Run II. Tracking and experimental data will be very useful.

2.5 *Beam Rounder, by A. Burov/FNAL*

This theoretical study provides a convenient formalism using circular modes to describe the beam motion. It can be used to express and enforce the conservation of the angular momentum. In this way, round beams may be provided at an interaction point from any emittance ratio. With this new invariant, the motion is essentially 2D where the diffusion in amplitude is minimized.

To support this approach, Y. Shatunov/Novossibirsk showed tracking results for the future VEPP 2000 in the case of beams rounded by betatron coupling. The blow-up of the core occurs at a significantly larger beam-beam parameter.

3 EVOLUTION OF THE UNDERSTANDING

3.1 *Issues in Novossibirsk/1989*

At this time, only the head-on beam-beam effect was an issue.

- Is $\xi = 0.02$ possible in only one IP?: Not an issue anymore. The ultimate limit seems on the side of the coherent effects (see J. Shi in the session on coherent effects).
- The diffusion in the tails need to be studied and measured: still true.
- The correction of the leading beam-beam effect (detuning) by octupoles should be studied. S. Temnykh/CESR mentions that this was done with some success in electron machines. For protons, the new ideas of an electron lens or a wire compensator are clearly superior.

3.2 *Issues in Montreux/1995*

- Matching the beam sizes is more important than a residual beam separation.
- Strong diffusion observed in HERA for amplitudes above 2 σ: That was not beam-beam.
- Long-range at LHC: the linear tune shift was an issue. The residual transverse separation, estimated to be up

to 1 σ, was not considered serious, based on experience in SPS, HERA and Tevatron: this does not seem consistent with reports in Geneva/1999.

3.3 Issues in Geneva/1999

- The non-linearity of the LR interactions is identified to be the major performance limit.
- A small transverse beam separation of 0.1 to 0.2 σ is reported to cause problems in several colliders (background, lifetime).
- Standardization of the simulation codes: It is noted that it is impossible to compare tracking results with many codes and as many input conventions. It is still the case. There is apparently no serious incentive (and framework) to make this effort.

3.4 Issues for this Workshop

It is quite clear that the hadron colliders entered the long-range interaction era which appears much more significant than anticipated. In electron machines, the main issue is the trade-off between flat and round beams. A side issue is the lack of consistence in the observations or interpretations of the effect of a residual beam separation at the IP's in Montreux/1995 and Geneva/1999. Experiments are needed to clarify this issue which is operationally important.

4 PROPOSED ACTIONS

We propose here a list of actions related to the main issues of this workshop.

- Measurement of the footprint due to the long-range interactions: a simple start to compare calculations and measurements and gain confidence.
- Phenomenology associated with the long-range interactions: Measurement of (lifetime, background, diffusion) versus (LR separation, number of LR's, tunes).
- Pacman Effect: bunch-by-bunch measurements of orbits, tunes, coupling, chromaticity, luminosity: is the effect as expected? how to handle all these data? usefulness.
- measurement of synchro-betatron coupling versus Xing angle with and without LR's.

This series of experiments would be best carried out on the Tevatron.

- Effect of a residual separation at the IP: what is tolerable? This experiment could be best carried out at RHIC.
- Compensation of the LR effect. The progress at Fermilab with the electron lens is significant and further experiments are of large interest for the community. The 'pulsed wire' method is under study at Cern. V. Shiltsev/FNAL proposes to test the idea (as much as possible) at the Tevatron. This is very much encouraged.
- Flat versus round beams (for electrons but as well hadrons): The studies on the Moebius machine are planned to be resumed. S. Temnykh challenges the community to help in finding a chromaticity correction scheme which works in this machine. When VEPP2000 will be ready, it will be an excellent place to study this issue.
- The report on the progress in understanding Daphne was very interesting and the community is looking forward to hear about the developments.
- Beam rounder: the concept is very interesting. Tracking and resonance calculations are necessary to evaluate the robustness of the scheme versus the imperfections which cannot be avoided in a real machine. These numerical studies are encouraged.

5 CONCLUSION

The performance of the new colliders are limited by new beam-beam issues (hadrons or electrons) with hardware consequences (Xing angle, corrections schemes, focusing doublets versus triplets). Theory and tracking provide a clue at the parameter dependence but cannot replace experiments, given the complexity of the problem. It becomes therefore necessary to launch a significant experimental study programme to improve the understanding and exploit the new ideas which are emerging.

6 ACKNOWLEDGEMENTS

Thanks to the organisers and the participants for a very interesting session. This report is based on on-the-fly workshop notes. Please be indulgent in case of minor mistakes. Otherwise, let me know.